Journal of Molecular Structure 1273 (2023) 134282

Contents lists available at ScienceDirect

Journal of Molecular Structure

journal homepage: www.elsevier.com/locate/molstr

In vitro cytotoxic effects, in silico studies, some metabolic enzymes inhibition, and vibrational spectral analysis of novel β-amino alcohol compounds

Ayca Tas[a,b], Burak Tüzün[c,*], Ali N. Khalilov[d,**], Parham Taslimi[e,f], Tugba Ağbektas[b], Nese Keklikcioglu Cakmak[g]

[a] Department of Nutrition and Diet, Faculty of Health Sciences, Sivas Cumhuriyet University, Sivas, Turkey
[b] Department of Biochemistry, Faculty of Medicine, Sivas Cumhuriyet University, Sivas, Turkey
[c] Plant and Animal Production Department, Technical Sciences Vocational School of Sivas, Sivas Cumhuriyet University, Sivas, Turkey
[d] "Composite Materials" Scientific Research Center, Azerbaijan State Economic University (UNEC), H. Aliyev Str. 135, Az 1063 Baku, Azerbaijan
[e] Department of Biotechnology, Faculty of Science, Bartin University, 74100 Bartin, Turkey
[f] Department of Chemistry, Faculty of Science, Istinye University, Istanbul, Turkey
[g] Department of Chemical Engineering, Faculty of Engineering, Sivas Cumhuriyet University, Sivas, 58140, Turkey

ARTICLE INFO

Article history:
Received 22 June 2022
Revised 25 September 2022
Accepted 4 October 2022
Available online 8 October 2022

Keywords:
β-amino alcohols
Cell culture
DFT
Molecular docking
Enzyme inhibition

ABSTRACT

In this study, an efficient single-step method for the preparation of β-amino alcohols (**1**–**3**) in aqueous media was applied. The aim was to investigate the cytotoxic activity of Compounds 1, 2 and 3 in neuroblastoma SH-SY5Y cell line and mouse fibroblast L-929 cell lines. Cytotoxic activities of compounds 1, 2 and 3 in this cell lines were also determined by MTT method. Cells were incubated with different concentrations of Compound 3 showed the highest cytotoxic activity in SHY5Y cells at an IC50 dose of 13.01±0.87 µM at 72 h compared to other compounds. Compound 3 was determined to have lower cytotoxic activity in L-929 cells. The chemical activities of the molecules against the B3LYP, HF, M062X level 3–21 g, 6–31 g, and SDD basis set with the Gaussian package program and biologically against the adenosine A(2A) receptor (PDB ID: 3PWH and 5NM4) proteins for neuroblastoma tumors cell with the Maestro Molecular modeling platform by Schrödinger were compared. Both experimental and theoretical NMR, UV–vis, and IR spectra of the studied molecules were compared. ADME/T analysis was performed to examine the drug properties of the molecules. Finally, these assayed for their activities against metabolic enzymes acetylcholinesterase and α-glucosidase. The most potent compounds against AChE were order compounds **3, 2** and **1** with K_i values of 35.88±6.61, 43.75±8.28, and 45.34±3.50 µM against AChE, respectively. The results indicated that all the synthesized compounds exhibited excellent inhibitory activities against mentioned enzymes as compared with standard inhibitors. These inhibitors may be candidates for drug design.

1. Introduction

The *vic*-amino alcohol is a prevalent motif in chiral auxiliaries, chiral ligands, chiral organocatalysts, drugs and natural products [1–4]. β-amino alcohols derived from natural amino acids have been widely used as a source of strong chirality. Chirality is an important property for drugs because of the different biological activities of the two enantiomers [5]. β-amino alcohols are used in the pharmaceutical industry as versatile intermediates in the preparation of many biologically active compounds [6]. They exhibit a broad spectrum of biological properties such as bactericide, fungicide, antiparasitic, enzyme inhibitory, antitumor, antileishmanial, antiarrhythmic activities [7–14]. Many of them found application in medical practice (Fig. 1a) [15,16]. Cytotoxic activity of various eugenol-based β-amino alcohol derivatives shows that some structural modifications resulted in enhanced cytotoxic activity toward cancer cells [17,18]. Considering this literature data and structural analogy with **1–3** compounds, some structure/activity relationships can be drawn, which may guide future structural improvements for anticancer agents. Consequently, herein, we disclose the results of the biological activity assessment of synthesized products **1**–**3** (Fig. 1b) [19].

* Corresponding author.
** Corresponding author.
E-mail addresses: theburaktuzun@yahoo.com.tr (B. Tüzün), xalilov_a@yahoo.com (A.N. Khalilov).

https://doi.org/10.1016/j.molstruc.2022.134282
0022-2860/

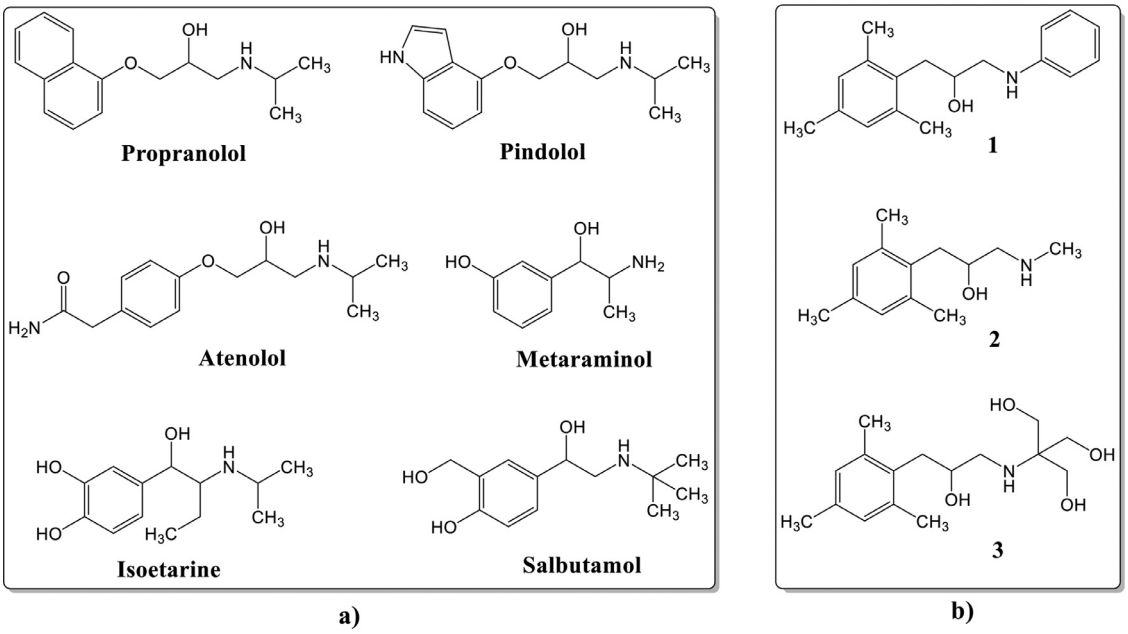

Fig. 1. The β-amino alcohol drugs (**a**); The β-amino alcohols used in the study (**b**).

Neuroblastoma (NB) is one of the most common tumors in children. NB usually originates from the sympathetic nervous system and adrenal glands. It can also occur from the abdomen, chest, spinal cord, and paraspinal ganglia [20]. NB accounts for approximately 9% of childhood cancers seen in one in 8000 live births. NB is seen in approximately 1 out of 105 children under the age of 15 in the world [21]. Diagnosis of cancer is 22 months on average, more than one third is under the age of 1, and more than 88% are diagnosed at the age of 5 [22]. The long-term survival rate of children with NB is only 5% to 15% [23]. Therefore, the 5-year overall survival probability of patients with high risk neuroblastoma is less than 50% [24]. In addition, these patients treated with chemotherapy are exposed to treatment-related sudden and long-term toxicities. NB cancer is a tumor that needs new treatment approaches. Toxicity studies have been carried out in cancer cell lines using anticancer drugs, different nanoparticles or various drugs [25].

Theoretical calculations are a widely used method for drug discovery today. With this method, it is possible to synthesize more effective and more active molecules [26,27]. Theoretical calculations are among the fastest and most accurate methods used to compare the activities of molecules. Among this method, the most known and most used programs are the Gaussian software program [28] and the Maestro Molecular modeling platform by Schrödinger [29]. Molecules can be modified to increase their activity of molecules by determining the active sites of molecules with theoretical calculations [30,31]. Many calculations were made in this study. The chemical activities of the molecules against the B3LYP, HF, M062X [32–34] level 3–21 g, 6–31 g, and SDD basis set with the Gaussian package program and biologically against the adenosine A(2A) receptor (PDB ID: 3PWH and 5NM4) [35,36] proteins for neuroblastoma tumors cell with the Maestro Molecular modeling platform by Schrödinger were compared. Both experimental and theoretical NMR, UV–vis, and IR spectra of the studied molecules were compared. Finally, ADME/T analysis was performed to examine the drug properties of the molecules.

α-Glucosidases (α-D-glucoside glucohydrolase, exo-$\alpha-$1,4-glucosidase) play a key role in carbohydrate metabolism in plants, animals and microorganisms. It is very common in microorganisms and has been characterized by purifying its extracellular, intracellular or cell-bound forms from various bacteria, yeasts and molds. Eukaryotic α-glucosidases isolated and purified; Examples are *Saccharomyces italicus* Y1225, a yeast, *Aspergillus niger*, a mold, and human lysosomal α-glucosidase [37,38]. Learning of cholinesterase (ChE) enzymes structure is essential for understanding their high catalytic efficacy as well as for the purpose, of rational drug design it is important to know everything related to these vital enzymes. ChEs are a family of enzymes that catalyzes the hydrolysis of ACh, a basic procedure taking into account the rebuilding of the cholinergic neuron. The two sorts of ChE are: (AChE; E.C. 3.1.1.7) and (BChE; E.C. 3.1.1.8). AChE is one of the well-known compounds, which plays an imperative part in the central nervous system. The availability of AChE crystal structures for distinct species with and without ligands gives a strong premise to structure-based plan of novel AChE inhibitors [39,40].

In this study, we aimed to determine some enzymes inhibition, in silico studies, and cytotoxicity potentials of these compounds on SH-SY5Y neuroblastoma and L-929 healthy mouse fibroblast cell lines by administering the newly synthesized Compound 1, 2 and 3 drugs.

2. Experimental

2.1. Chemistry section

2.1.1. General

Melting points were determined by a Stuart SMP30 melting point apparatus and are uncorrected. The ^{1}H and ^{13}C NMR spectra of known compounds were recorded on a Bruker Avance II + 300 (UltraShieldTM Magnet) instrument in DMSO at 300 MHz. All the chemicals were purchased by chemical producers Merck (Darmstadt, Germany) and Fluka (Buchs, Switzerland) and used without further purification.

2.1.2. General procedure for the synthesis of compounds (1–3)

To a 1–chloro-3-mesitylpropan-2-ol (10 mmol) in water (20 mL) an amine (30 mmol) was added and was vigorously stirred at 90 °C temperature for 4–24 h until the reaction mixture become homogeneous. Then the reaction mixture was cooled down. Then the precipitated white solid products were separated by filtration and recrystallized from carbon tetrachloride [19,41].

2.1.3. 1-Mesityl-3-(phenylamino)propan-2-ol (1)

Yield 36%; Mp 123–124 °C; ^{1}H NMR (300 MHz, DMSO-D_6): 2.20 (s, 3H, CH_3); 2.28 (s, 6H, 2CH_3); 2.75 (d, 2H, CH_2-Ar); 3.00 (m, 2H, N–CH_2); 3.85 (m, 1H, CH); 4.77 (d, 1H, OH); 5.05 (t, 1H, NH); 6.49 (m, 3H, 3CH_{ar}); 6.74 (s, 2H, 2CH_{ar}); 7.02 (d, 2H, 2CH_{ar}); ^{13}C NMR (300 MHz, DMSO-D_6): 20.90 (2CH_3-Ar); 21.00 (CH_3-Ar); 36.20 (CH_2-Ar); 49.90 (N–CH_2); 69.90 (CHO); 113.1 (2CH_{ar}); 117.8 (1CH_{ar}); 128.9 (4CH_{ar}); 134.5 (C_{ar}-CH_2); 136.7 (C_{ar}-CH_3); 137.8 (2C_{ar}-CH_3); 148.9 (C_{ar}-NH).

2.1.4. 1-Mesityl-3-(methylamino)propan-2-ol (2)

Yield 67%; Mp 104–106 °C; ^{1}H NMR (300 MHz, DMSO-D_6): 2.15 (s, 3H, CH_3); 2.25 (s, 6H, 2CH_3); 2.52 (s, 3H, N–CH_3); 2.62 (m, 2H, H_2C-Ar); 2.82 (m, 2H, CH_2–N); 3.15 (s, 2H, NH+OH); 4.10 (m, 1H, CH); 6.75 (s, 2H, 2CH_{ar}). ^{13}C NMR (300 MHz, DMSO-D_6): 20.00 (2CH_3-Ar); 20.10 (CH_3-Ar); 33.41 (CH_3–N); 37.30 (CH_2-Ar); 55.22 (CH_2–N); 68.40 (CHO); 129.20 (2CH_{ar}); 132.30 (C_{ar}-CH_2); 134.7 (C_{ar}-CH_3); 136.7 (2C_{ar}-CH_3).

2.1.5. 2-((2-Hydroxy-3-mesitylpropyl)amino)–2-(hydroxymethyl)propane-1,3-diol (3)

Yield 65%; Mp 105–106 °C; ^{1}H NMR (300 MHz, DMSO-D_6): 2.17 (s, 3H, CH_3); 2.24 (s, 6H, 2CH_3); 2.54 (d, 2H, CH_2-Ar); 2.63 (d, 2H, CH_2–N); 3.31 (s, 6H, 3CH_2–O); 3.51 (s, 3H, OH); 3.55 (m, 1H, CH–O); 4.30 (s, 1H, NH); 4.69 (s, 1H, OH); 6.77 (s, 2H, 2CH_{ar}). ^{13}C NMR (300 MHz, DMSO-D_6): 20.62 (2CH_3-Ar); 20.90 (CH_3-Ar); 35.50 (CH_2-Ar); 47.7 (CH_2–N); 59.82 (C_{tert}-N); 61.45 (3CH_2–O); 71.62 (CHO); 128.98 (2CH_{ar}); 133.86 (C_{ar}-CH_2); 134.53 (C_{ar}-CH_3); 136.84 (2C_{ar}-CH_3).

2.2. Cytotoxicity activity assay

Compounds 1, 2 and 3 were administered to cell lines and their cytotoxic activity was analyzed using the MTT method. These cell lines were grown in DMEM (Dulbecco's Modified Eagle Medium) medium containing 1% penicillin-streptomycin and 10% fetal bovine serum (FBS). SH-SY5Y and L-929 cell lines were manufactured at 37 °C, 95% moisture and 5% CO_2. Cells (1 × 105/well) were then sowed into 96 well plates after 24 h of growth and compounds were applied to the cells at 8 different doses ranging from 1 to 100 µM. Cells were incubated with these drugs for 24, 48 and 72 h. After incubation of cells, 10 µL of MTT was added to each well. After the addition of MTT, incubation was done at 37 °C for 3 h in an environment containing 5% CO_2. MTT was aspirated from the cells. Then, 100 µL of dimethyl sulfoxide (DMSO) was attached to each well and incubated for 15 min. In order to determine the cytotoxic activity of the cells, absorbance values were read with a microplate reader at 570 nm. Data were analyzed using the GraphPad Prism method. Then graphics were created.

2.3. Morphological examination of cells

10 mM Compounds 1, 2 and 3 were added to each of the cells. The morphology of the cells after the applied dose was examined on the device at 20X magnification (ZEISS Axio Vert.A1).

2.4. Statistical analysis

In the cytotoxic activity determination study in cell lines, each compound was performed in triplicate. Results are given as mean±SEM. Study data were analyzed by one-way ANOVA method. Differences were considered significant. The statistical significance levels of the doses are given on the columns in 1–6 figures ($^*p<0.05$, ** $p<0.01$ and $^{**}p<0.0001$).

2.5. Theoretical calculation

Theoretical calculations provide important information about the chemical and biological properties of molecules. Many quantum chemical parameters are obtained from theoretical calculations. The calculated parameters are used to explain the chemical activities of the molecules. Many programs are used to calculate molecules. These programs are Gaussian09 RevD.01 and GaussView 6.0 [28,42] By using these programs, calculations were made in B3LYP, HF, M06–2X [32–34] methods with the 6–31++g(d,p) basis set. As a result of these calculations, many quantum chemical parameters have been found. each parameter describes a different chemical property of molecules. These parameters are HOMO (Highest Occupied Molecular Orbital), LUMO (Lowest Unoccupied Molecular Orbital), ΔE (HOMO-LUMO energy gap), chemical potential (μ), electrophilicity (ω), chemical hardness (η), global softness (σ), Many parameters such as nucleophilicity (ε), dipole moment, energy value are calculated [43–45].

$$\chi = -\left(\frac{\partial E}{\partial N}\right)_{\upsilon(r)} = \frac{1}{2}(I+A) \cong -\frac{1}{2}(E_{HOMO}+E_{LUMO})$$

$$\eta = -\left(\frac{\partial^2 E}{\partial N^2}\right)_{\upsilon(r)} = \frac{1}{2}(I-A) \cong -\frac{1}{2}(E_{HOMO}-E_{LUMO})$$

$$\sigma = 1/\eta \;\; \omega = \chi^2/2\eta \;\; \varepsilon = 1/\omega$$

Molecular docking calculations are performed to compare the biological activities of molecules against biological materials. The program developed by Maestro Molecular modeling platform (version 12.8) by Schrödinger [21] was used for molecular docking calculations. Calculations are made up of several steps. Each step is done differently. In the first step, the protein preparation module [46] was used in the preparation of proteins. In this module, the active sites of the proteins were determined. In the next step, the studied molecules are prepared. First, the molecules are optimized in the gaussian software program, then the LigPrep module [47] is prepared for calculations using optimized structures. The Glide ligand docking module [48] was used to examine the interactions between the molecules and the cancer protein after preparation. Calculations were made using the OPLS4 method in all calculations. Finally, ADME/T analysis (absorption, distribution, metabolism, excretion and toxicity) will be performed to examine the drug potential of the studied molecules. The Qik–prop module [49] of the Schrödinger software was used to predict the effects and reactions of molecules in human metabolism.

2.6. Enzymes assays

ChE inhibitory activities of the title compounds against AChE was determined by Ellman's method [50]. In this assay, AChE from electric eel (*Electrophorus electricus*) and BChE from equine serum were used [51]. α-Glucosidase inhibitory activity of novel derivatives was determined according to the reported method by Tao et al. [52].

3. Results and discussion

β-Amino alcohols were resynthesized according to the literature [19]. The formulas of the compounds used in the study are given in Fig. 1b.

In present study, cytotoxic activities of Compounds 1, 2 and 3 were evaluated in Table 1 and Figs. 2–4. The percentages of survival of cells after administration of the compounds were calculated and compared with each other. IC_{50} doses of compounds applied to cells were found to be more effective in SH-SY5Y cells.

Table 1
Comparison of IC50 values of Compounds 1, 2 and 3 in cell lines.

	SH-SY5Y IC_{50} (μM±SD*)			L929		
Drugs	24h	48h	72h	24h	48h	72h
Compound **1**	≥100	42,23±0,21	35,97±1,67	≥100	≥100	≥100
Compound **2**	64,76±1,46	44,53±1,98	36,12±3,51	78,87±3,76	52,05±1,07	47,71±1,48
Compound **3**	25,96±1,23	16,71±2,33	13,01±0,87	91,32±1,99	82,77±2,79	52,14±4,32

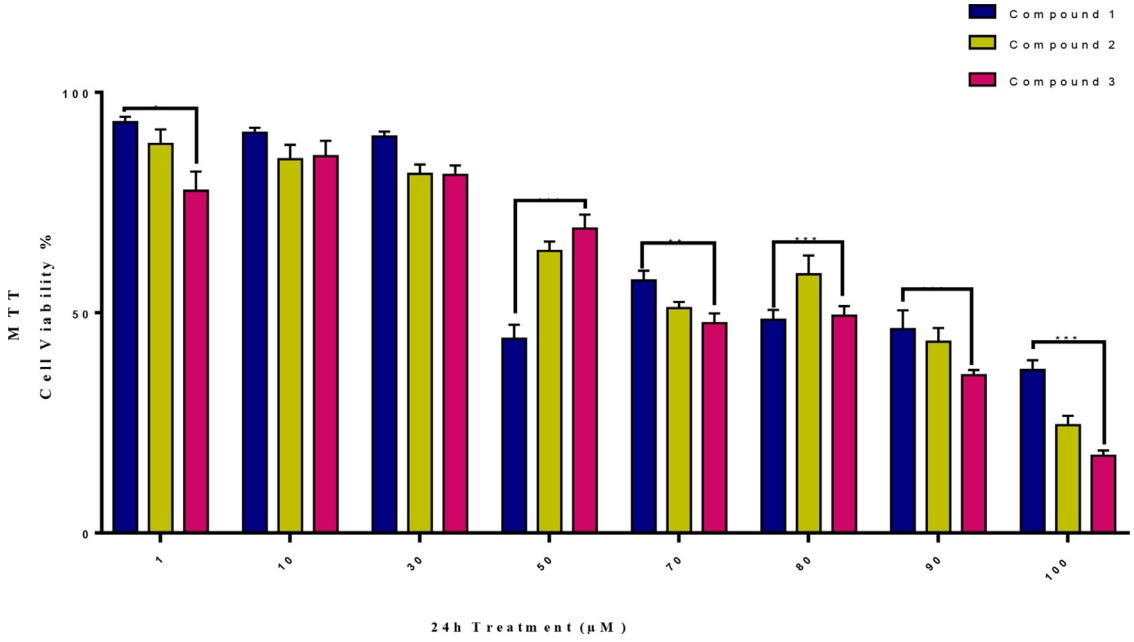

Fig. 2. Determination of the cytotoxic activity of compounds **1, 2** and **3** in SH-SY5Y cells. Activities of compounds after 24-hour incubation at concentrations ranging from 1 to 100 µM.

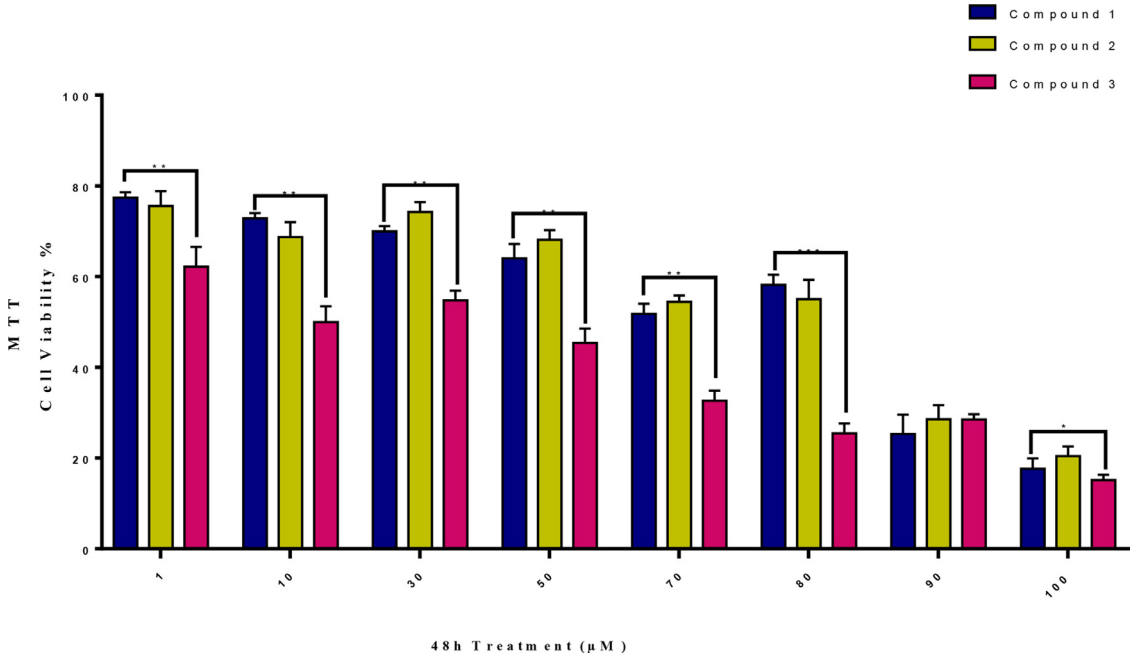

Fig. 3. Determination of the cytotoxic activity of compounds **1, 2** and **3** in SH-SY5Y cells. Activities of compounds after 48-hour incubation at concentrations ranging from 1 to 100 µM.

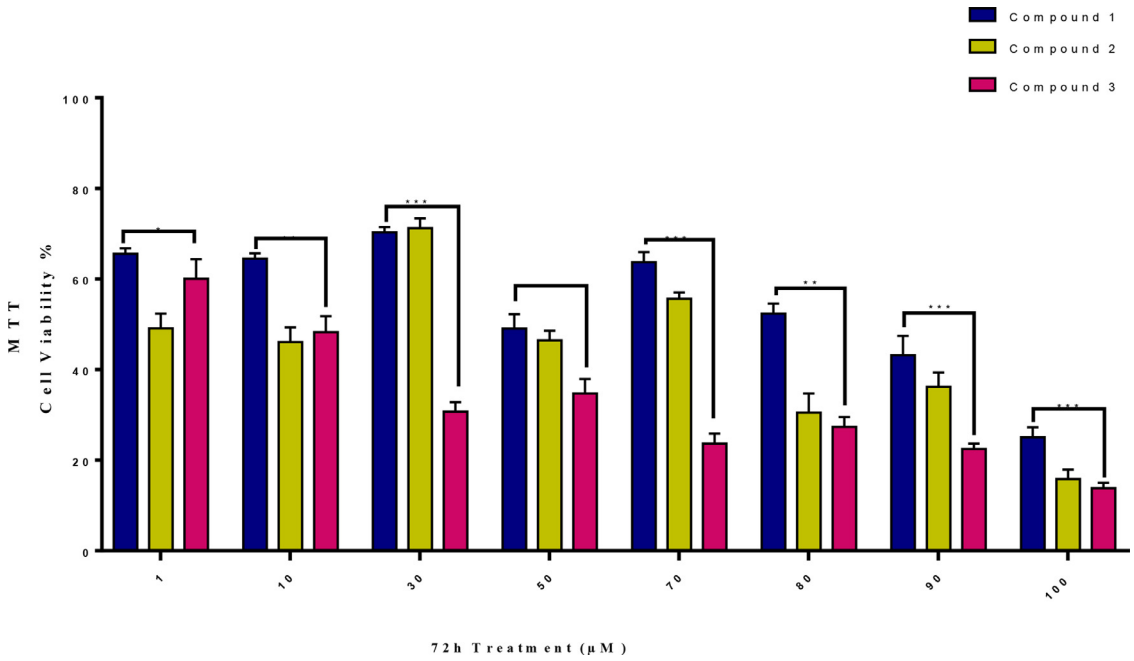

Fig. 4. Determination of the cytotoxic activity of compounds **1, 2** and **3** in SH-SY5Y cells. Activities of compounds after 72-hour incubation at concentrations ranging from 1 to 100 µM.

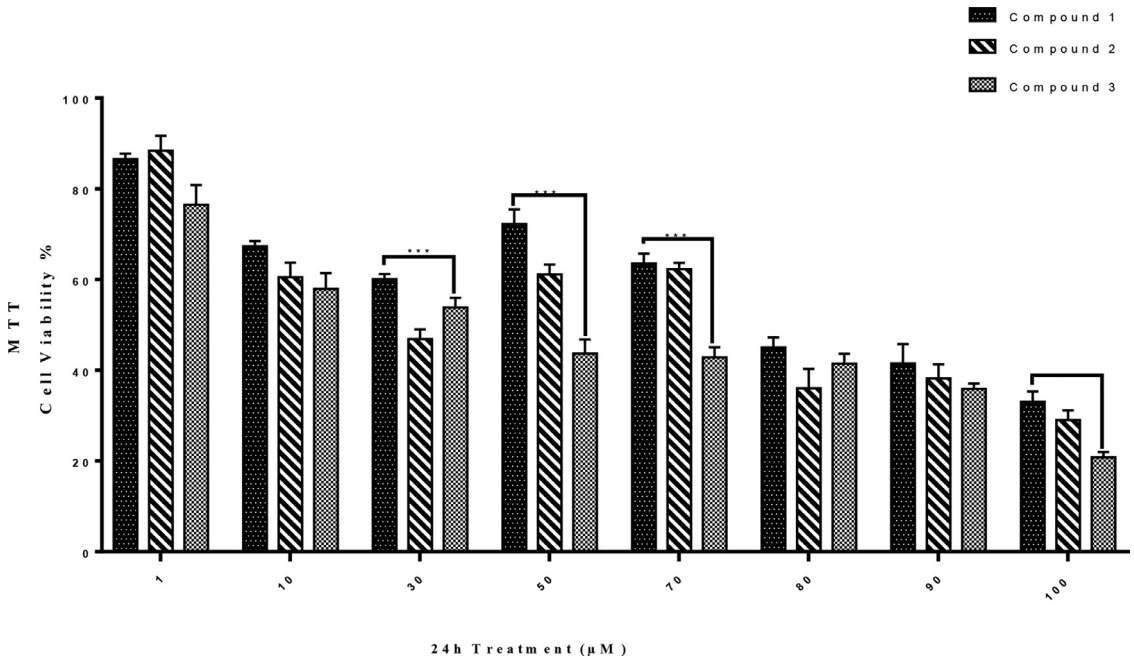

Fig. 5. Cytotoxicity activity of compounds in L-929 cells. Doses of compounds in the dose range of 1–100 µM were administered over 24 h.

Cytotoxic activity on compounds cells was found to be most active at 72 h over the three time periods. Compound 3 showed the highest cytotoxic activity amongst the compounds performed to SH-SY5Y cells. Compound 3 was found to have the highest cytotoxic activity at 72 h in SH-SY5Y cells with an IC50 dose of 13.01±0.87 µM. The IC50 concentration of Compound 3 in the L-929 cell line is 52.14 ± 4.32 µM for 72 h (Table 1). In SH-SY5Y cancer cells, Compound 2 had the most active cytotoxicity at 72 h and the IC_{50} concentration was 36.12 ± 3.51 µM, while the cytotoxicity of Compound 1 was found to be 35.97 ± 1.67 µM at 72 h (Table 1). Morphological analyzes were performed 24 h after the administration of Compounds 1, 2 and 3 at a dose of 10 µM to SH-SY5Y and L-929 cells (Fig. 5-8).

Compounds 1, 2 and 3 were found to significantly alter the morphology of the cells in SH-SY5Y cells compared to the control group. All three compounds were found to produce more morphological changes in SH-SY5Y cells compared to L-929 cells. Compound 3 was found to be more effective than the compounds applied to the cells. In one study, different concentrations of paclitaxel and docetaxel ranging from 0.1 nM to 10 µM were administered to SH-SY5Y cells (3, 6, 12, 24, 48, and 72 h) and cytotoxic activities were determined. It was determined that paclitaxel and docetaxel drugs showed antineoplastic activity in SH-SY5Y cell

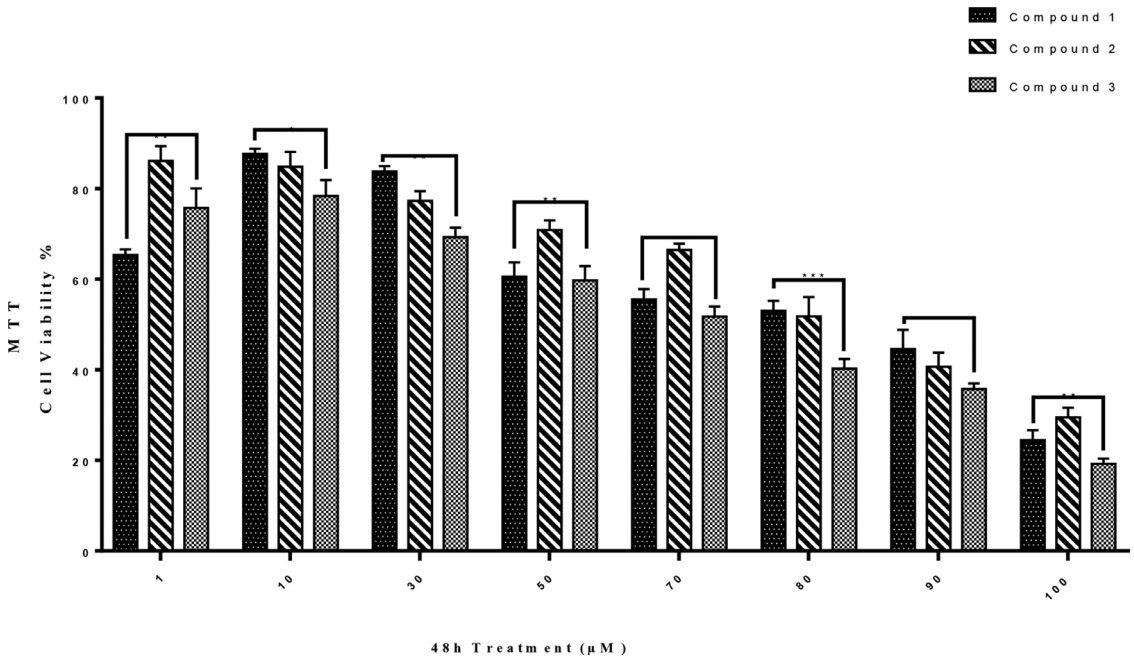

Fig. 6. Cytotoxicity activity of compounds in L-929 cells. Doses of compounds in the dose range of 1–100 µM were administered over 48 h.

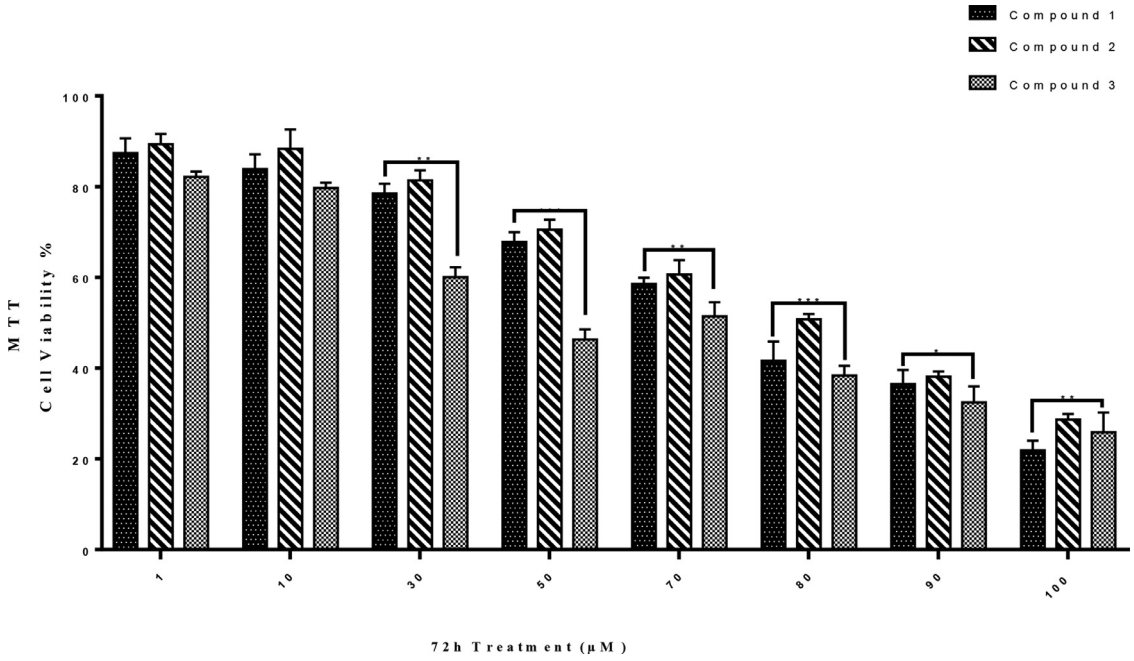

Fig. 7. Cytotoxicity activity of compounds in L-929 cells. Doses of compounds in the dose range of 1–100 µM were administered over 72 h.

lines. Therefore, our study results suggest that Compound 3 may be a drug candidate when compared with these results [53].

Comparing the activities of molecules as a result of theoretical calculations is both fast and easy. In the calculations made with the Gaussian package program, many quantum chemical calculations of the molecules were made. Among these calculated quantum chemical parameters, the most important parameters are Highest Occupied Molecular Orbital (HOMO) and Lowest Unoccupied Molecular Orbital (LUMO), which explain the electron donating properties of molecules. this is used to explain the activities of molecules. The activity of the molecule with the most positive numerical value of the Highest Occupied Molecular Orbital parameter of the molecules is higher than the activity of other molecules [54]. On the other hand, the activity of the molecule with the most negative numerical value of the Lowest Unoccupied Molecular Orbital parameter of the molecules is higher than the activity of other molecules [55]. As a result of the calculations, many parameters were calculated. From these calculations, it is seen that the compound 3 has the highest value in all basis sets, according to the numerical value of the HOMO parameter of the molecules. These parameters are used to explain the activities of molecules, since electron transfer occurs between molecules. Apart from these two parameters, many parameters of the molecular are calculated. All of these parameters are given in Table 2. but since many parameters are calculated from these two parameters, a similar ranking is obtained.

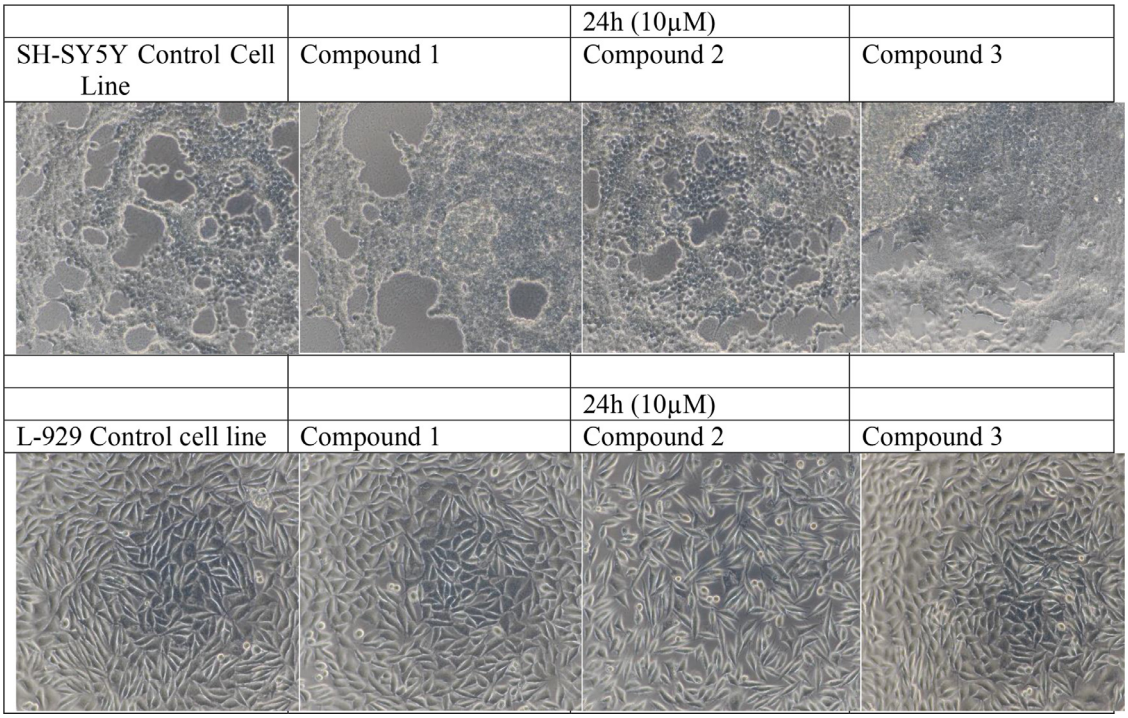

Fig. 8. Morphological changes of cells after 24 h of incubation with 10 μM dose of Compounds **1, 2** and **3**.

Table 2
The calculated quantum chemical parameters of molecules.

	E_{HOMO}	E_{LUMO}	I	A	ΔE	η	Σ	X	Pİ	ω	ε	dipol	Energy
B3LYP/3–21 g LEVEL													
1	−5.7950	−0.0229	5.7950	0.0229	5.7721	2.8861	0.3465	2.9089	−2.9089	1.4660	0.6821	3.6024	−22,446.4004
2	−5.6948	0.5510	5.6948	−0.5510	6.2459	3.1229	0.3202	2.5719	−2.5719	1.0590	0.9442	4.3040	−17,258.7453
3	−5.5697	0.7274	5.5697	−0.7274	6.2970	3.1485	0.3176	2.4212	−2.4212	0.9309	1.0742	5.8913	−26,553.8927
B3LYP/6–31 g LEVEL													
1	−5.4197	0.0648	5.4197	−0.0648	5.4845	2.7422	0.3647	2.6775	−2.6775	1.3071	0.7650	1.9350	−22,564.4895
2	−5.7457	0.4642	5.7457	−0.4642	6.2100	3.1050	0.3221	2.6407	−2.6407	1.1230	0.8905	3.8184	−17,349.1995
3	−5.5923	0.6071	5.5923	−0.6071	6.1993	3.0997	0.3226	2.4926	−2.4926	1.0022	0.9978	5.1803	−26,692.8085
B3LYP/SDD LEVEL													
1	−5.5493	−0.2555	5.5493	0.2555	5.2937	2.6469	0.3778	2.9024	−2.9024	1.5913	0.6284	1.9488	−22,566.8587
2	−5.8407	0.2672	5.8407	−0.2672	6.1079	3.0540	0.3274	2.7867	−2.7867	1.2715	0.7865	3.9095	−17,351.2589
3	−5.6312	0.4963	5.6312	−0.4963	6.1275	3.0638	0.3264	2.5674	−2.5674	1.0757	0.9296	7.0284	−26,697.2006
HF/3–21 g LEVEL													
1	−8.1891	3.8779	8.1891	−3.8779	12.0670	6.0335	0.1657	2.1556	−2.1556	0.3851	2.5970	3.4673	−22,297.3093
2	−8.1480	4.3675	8.1480	−4.3675	12.5154	6.2577	0.1598	1.8903	−1.8903	0.2855	3.5027	3.8251	−17,143.4508
3	−7.9599	4.5637	7.9599	−4.5637	12.5236	6.2618	0.1597	1.6981	−1.6981	0.2303	4.3429	5.6610	−26,386.4669
HF/6–31 g LEVEL													
1	−7.7659	3.8956	7.7659	−3.8956	11.6615	5.8308	0.1715	1.9352	−1.9352	0.3211	3.1140	1.6192	−22,413.4968
2	−8.0541	4.2896	8.0541	−4.2896	12.3437	6.1719	0.1620	1.8822	−1.8822	0.2870	3.4842	3.5330	−17,232.2833
3	−7.8233	4.5490	7.8233	−4.5490	12.3723	6.1861	0.1617	1.6372	−1.6372	0.2166	4.6159	6.7771	−26,522.7558
HF/SDD LEVEL													
1	−7.6639	3.5982	7.6639	−3.5982	11.2621	5.6310	0.1776	2.0328	−2.0328	0.3669	2.7253	2.4453	−22,415.9758
2	−8.1553	3.9675	8.1553	−3.9675	12.1228	6.0614	0.1650	2.0939	−2.0939	0.3617	2.7649	3.6623	−17,234.4563
3	−7.9262	4.2096	7.9262	−4.2096	12.1358	6.0679	0.1648	1.8583	−1.8583	0.2845	3.5144	6.8172	−26,527.0594
M062X/3–21 g LEVEL													
1	−7.1626	0.9731	7.1626	−0.9731	8.1357	4.0679	0.2458	3.0948	−3.0948	1.1772	0.8495	3.6389	−22,436.3641
2	−7.0718	1.5475	7.0718	−1.5475	8.6193	4.3096	0.2320	2.7621	−2.7621	0.8851	1.1298	4.3193	−17,250.7319
3	−7.1923	1.4588	7.1923	−1.4588	8.6511	4.3256	0.2312	2.8667	−2.8667	0.9500	1.0527	2.4473	−26,542.5545
M062X/6–31 g LEVEL													
1	−7.1403	0.8572	7.1403	−0.8572	7.9975	3.9987	0.2501	3.1416	−3.1416	1.2341	0.8103	3.3765	−22,554.5088
2	−7.1041	1.4155	7.1041	−1.4155	8.5197	4.2598	0.2348	2.8443	−2.8443	0.9496	1.0531	3.7647	−17,341.3215
3	−6.9839	1.5279	6.9839	−1.5279	8.5118	4.2559	0.2350	2.7280	−2.7280	0.8743	1.1438	4.7402	−26,681.6136
M062X/SDD LEVEL													
1	−6.9210	0.6615	6.9210	−0.6615	7.5825	3.7913	0.2638	3.1297	−3.1297	1.2918	0.7741	2.0955	−22,557.5883
2	−7.2045	1.2063	7.2045	−1.2063	8.4108	4.2054	0.2378	2.9991	−2.9991	1.0694	0.9351	3.9016	−17,343.7429
3	−6.9411	1.4760	6.9411	−1.4760	8.4171	4.2085	0.2376	2.7326	−2.7326	0.8871	1.1272	7.4911	−26,686.5421

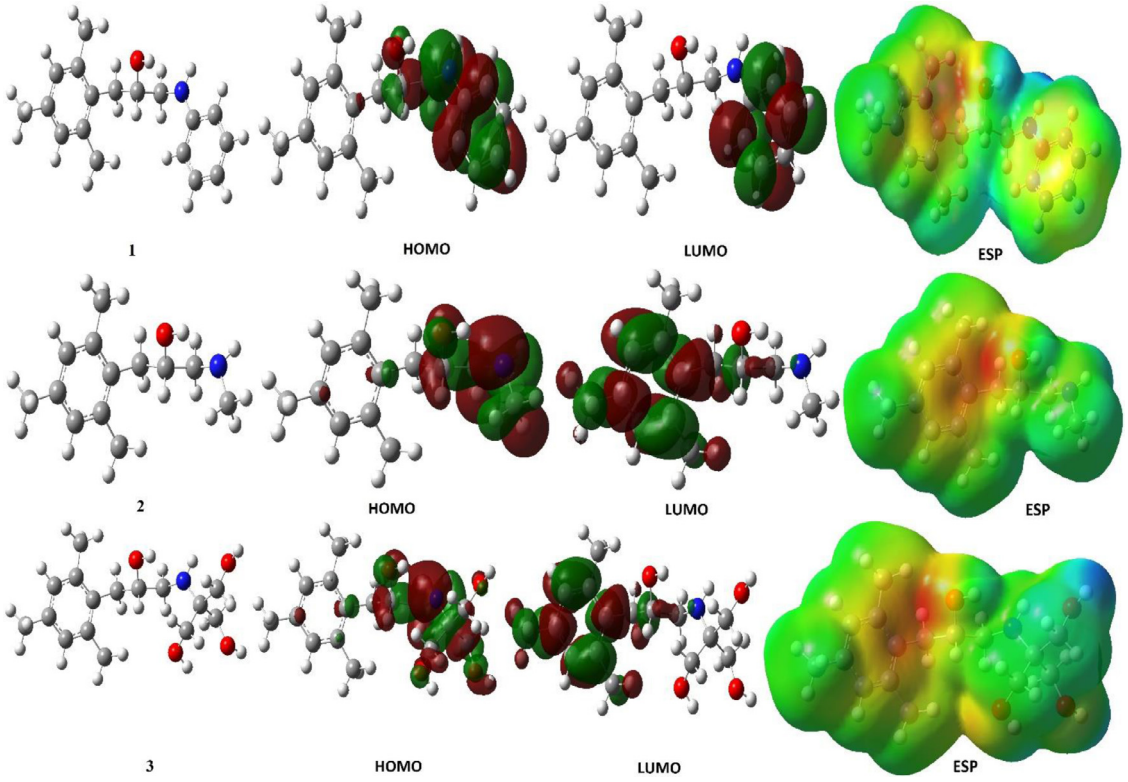

Fig. 9. Shapes of optimized structure, HOMO, LUMO and ESP of all molecule.

On the other hand, it is known that molecules with the lowest numerical value of the HOMO-LUMO energy gap value have the highest chemical activity [56]. In the calculations, it is known that the molecule with the lowest numerical value of the HOMO-LUMO energy gap parameter of the molecules has higher activity than other molecules.

Although molecules have many calculated parameters, few of them can be visualized. these are given in Fig. 9. are the optimized shapes of the first visual molecules. Using this optimized structure, it is seen on which atoms the HOMO and LUMO orbitals of the molecules are located. In the last relative, electrostatic potential (ESP) images are given, in which electron charge distributions of molecules are given. It has been understood that this visual molecule has two active points. The red regions are the regions with the highest electron density, which are the regions with the highest electron donating potential [57,58]. However, the blue regions, which are the regions with the lowest electron density, are the regions with the highest electron acceptability potentials.

3.1. Nuclear magnetic resonance (NMR) spectra

Nuclear magnetic resonance spectroscopy of molecules, generally abbreviated NMR spectroscopy, is a research technique that uses certain magnetic properties of atomic nuclei. It determines the physical and chemical properties of the atoms or molecules in it. NMR Spectroscopy gives information about the skeleton of the molecule, depending on the magnetic character of the atomic nucleus. Other spectroscopic methods deal with electrons, NMR Spectroscopy with the nucleus [59]. NMR analysis was done at room temperature on a Bruker Avance II+300 (UltraShieldTM Magnet) spectrometers operating at 300.130 and 75.468 MHz for proton and carbon-13, respectively in experimental analyses in Figure S4-S9. On the other hand, Chemical shift values of carbon and hydrogen atoms of all compound were calculated by using the gage-independent atomic orbital (GIAO) method [60] in theoretical analysis. The NMR spectrum of the all compound was calculated on the HF/6–31++*g* basis set. The calculated chemical shift values are given in Table S1-S3. The chemical shift values calculated with the experimental chemical shift values obtained were plotted. The chemical shift values of carbon and hydrogen atoms in each molecule in gas phase, methanol phase, and DMSO phase were calculated theoretically. Labeling of atoms is given in Figure S1-S3. The correlation coefficient values (R^2) were calculated for each molecule. It can be seen that this value is very close to 1. R^2 values for each molecule in all three phases are 0.99 in Figs. 10–12. When this table and graphic is examined in detail, it is seen that carbon atoms with a chemical shift value of 20–70 ppm are aliphatic carbon atoms, while the others are aromatic carbons [61]. On the other hand, it is seen that hydrogen atoms with chemical shift values between 7.28–8.18 ppm are attached to the aromatic ring [62]. However, it is seen that hydrogen atoms with a chemical shift value of 2.28–4.14 ppm are hydrogen atoms attached to aliphatic carbons [63].

3.2. Infrared spectroscopy

Infrared (IR) spectroscopy spectra of molecules is a characterization method obtained from the vibrations of atoms in the molecule. This spectrum method is the measurement of the interaction of infrared radiation with the molecule through absorption, emission or reflection [64]. It is used to study and identify solid, liquid or gaseous chemical substances or functional groups. These vibrations occurring in molecules provide the formation of IR spectra. The IR spectrum of the molecules was calculated on the HF/6–31++*g* basis set. Many vibrations are observed in the molecule. Both experimental and theoretical IR spectrums were obtained for the compound 1, 2, and 3. In Figs. 13–15, both spectra are compared. The red colored spectrum is the theoretical spectrum and the blue colored spectrum is the experimental spectrum.

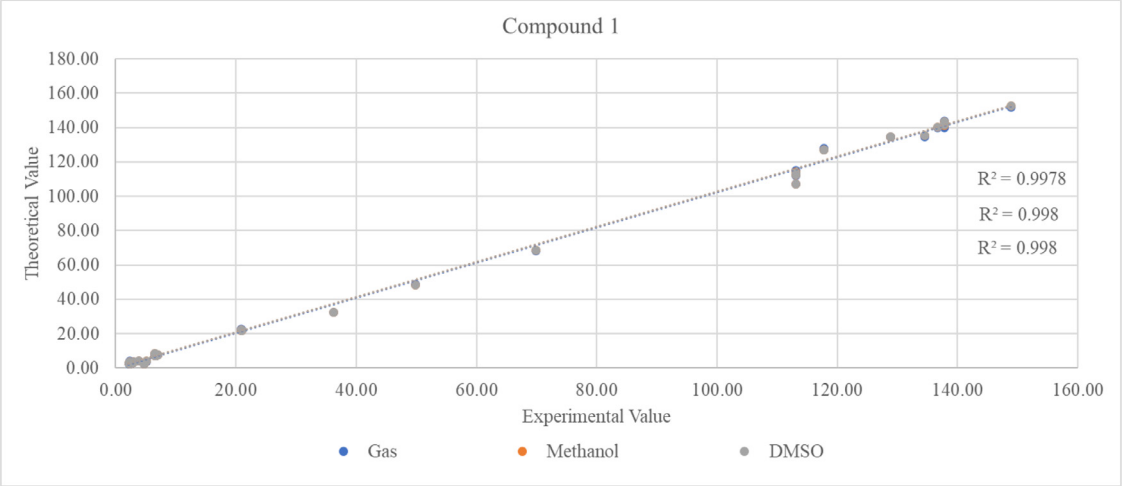

Fig. 10. Experimental and theoretical graph of all chemical shift values of compound **1**.

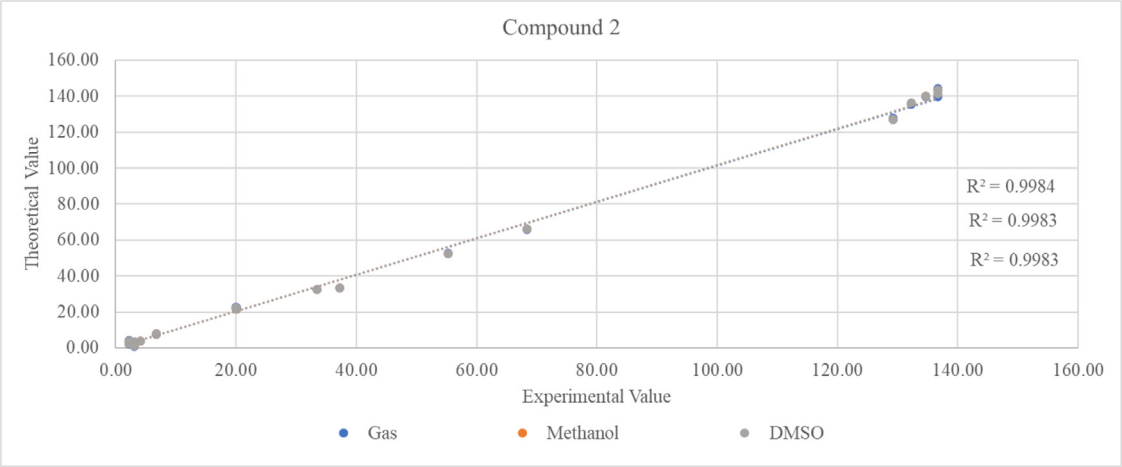

Fig. 11. Experimental and theoretical graph of all chemical shift values of compound **2**.

Each molecule was pressed into potassium bromide pellets and then used for the purpose of examining the functional groups by means of a Fourier transform infrared spectrophotometer (FTIR: Bruker: Tensor II) in the interval ranging from 4000 to 500 cm^{-1}. The spectra of the prepared samples were recorded by employing a UV–Vis spectrophotometer (UV-2600, Shimadzu, Japan) in the range of 200–800 nm. It is crucial to study the functional groups, combinations of various substances, and possible variations in the structure of substances for the material's structure. FTIR is frequently employed for the analysis and description of a material's structure and investigation of the interaction of various groups. FTIR analyses were conducted with the aim of observing functional groups in the current study.

The N–H stretches of amines are present in the 3300–3000 cm^{-1} region [65]. The mentioned bands are weaker and sharper in comparison with the bands of the alcohol O–H stretches occurring in the identical region. Secondary amines (R_2NH) exhibit a single weak band in the region of 3300–3000 cm^{-1}. Because they have a single N–H bond. The peaks that correspond to 2° amine found in all three molecules are observed at 3350–3310 cm^{-1}. O–H and N–H stretching vibrations are defined by absorption peaks in the region of 3700–3100 cm^{-1}. Peaks belonging to O–H tend to be at higher wavenumbers. O–H bands are wider than hydrogen bond formation causes the broadening of peaks and shifts them to lower wavenumbers. O–H and N–H overlapping occur at identical wavelengths in all three molecules. The peak observed at ~3300 in compound 3 is broader than the others and originates from the O–Hs in the molecule.

The molecules cause C–H modes, including stretching, in-plane and out-of-plane bending vibration. Aromatic compounds usually show multiple weak bands in the 3000– 3100 cm^{-1} [66] region because of aromatic C–H stretching vibrations. The C–H in-plane bending frequencies occur in the 1000– 1300 cm^{-1} range, while C–H out-of-plane bending vibration occurs in the 750–1000 cm^{-1} range for aromatic compounds [67,68]. The aromatic C–H stretching bands are revealed to be weak, which is caused by the decreased dipole moment due to a reduction in negative charge on the carbon atom. There are two types of CH modes in the molecule, including CH modes in the ring and the CH_3 modes of substituted methyl groups.

There are three methyl groups in the mesitylene molecule in the first, third, and fifth positions. For benzene derivatives that contain a CH_3 group, two bands with asymmetric and symmetric stretching appear. The asymmetric stretching for the CH_3 and CH_2 groups has a higher magnitude compared to the symmetric stretching [69]. The CH stretching vibration of methyl groups occurs at frequencies lower than the frequencies of the aromatic ring (3000–3100 cm^{-1}). The asymmetric and symmetric stretching modes of the methyl group attached to the benzene ring are generally downshifted because of electronic impacts and are fore-

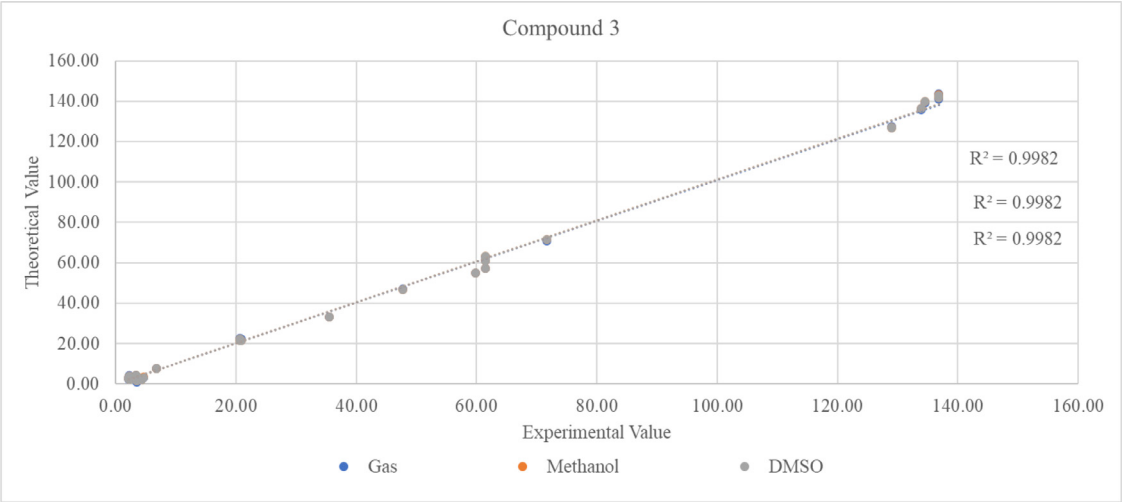

Fig. 12. Experimental and theoretical graph of all chemical shift values of compound **3**.

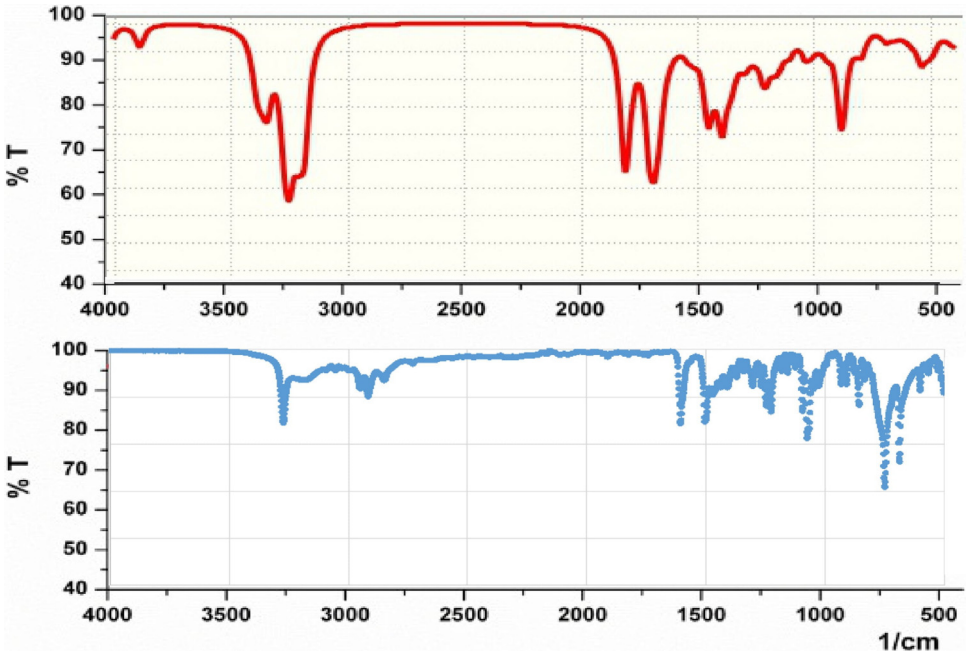

Fig. 13. IR spectra of compound **1**.

seen around 2990, 2940 cm^{-1} asymmetric and 2860 cm^{-1} symmetric stretching vibrations. In the current study, the examined wavenumbers were recorded at 2965, 2946, 2922 cm^{-1} asymmetric and 2918, 2851,2855, 2730 cm^{-1} symmetric stretching vibrations, which is identical in all three molecules, and the experimental values represent very good consistent calculated data. The ring stretching vibrations are essential and represent the important characteristic of the aromatic ring itself. The CC stretching vibration modes in the phenyl ring usually take place in the 1430–1625 cm^{-1} region in all three molecules. The wavenumbers identified in the FT-IR spectrum at 1605 and 1503 cm^{-1} were assigned to C = C stretching vibrations in molecule 1 [70].

The C–CH_3 vibrations represent significant modes for the molecules with methyl groups. The said modes are usually contaminated with C–H in-plane bending vibration [71,72]. The active fundamental mode revealed as C–CH_3 was determined at 1226 cm^{-1} in FT-IR. There is good agreement between the C–CH_3 stretching mode and the calculated wavenumber.

The presence of the ring stretching modes of mono-substituted benzene is foreseen in the 1620–1285 cm^{-1} range [73]. For compound 1, the phenyl ring stretching modes are detected at 1600, 1503, 1471 cm^{-1} in the IR spectrum. There is a considerably high overlap between regions. Therefore, the deformations frequently overlap a lot of molecules. For the hydroxyl group, three normal vibrations, such as the stretching vibration υOH, in-plane and out-of-plane deformations δOH and γOH, are ensured by the OH group. The in-plane OH deformation [74–76] is predicted in the 1440 ± 40 cm^{-1} region. The stretching of hydroxyl group C–O is foreseen in the 1220 ± 40 cm^{-1} region [29–31]. Varghese et al. stated υOH at 3633 and δOH at 1345 cm^{-1} in theory and CO stretching at 1255 cm^{-1} in IR spectra. The out-of-plane deformation is usually predicted in the 650 ± 80 cm^{-1} region [77]. For the compounds, OH modes are assigned at 3466 (stretching), 1407 (in-plane deformation), and 631 cm^{-1} (out-of-plane deformation) experimentally and in theory.

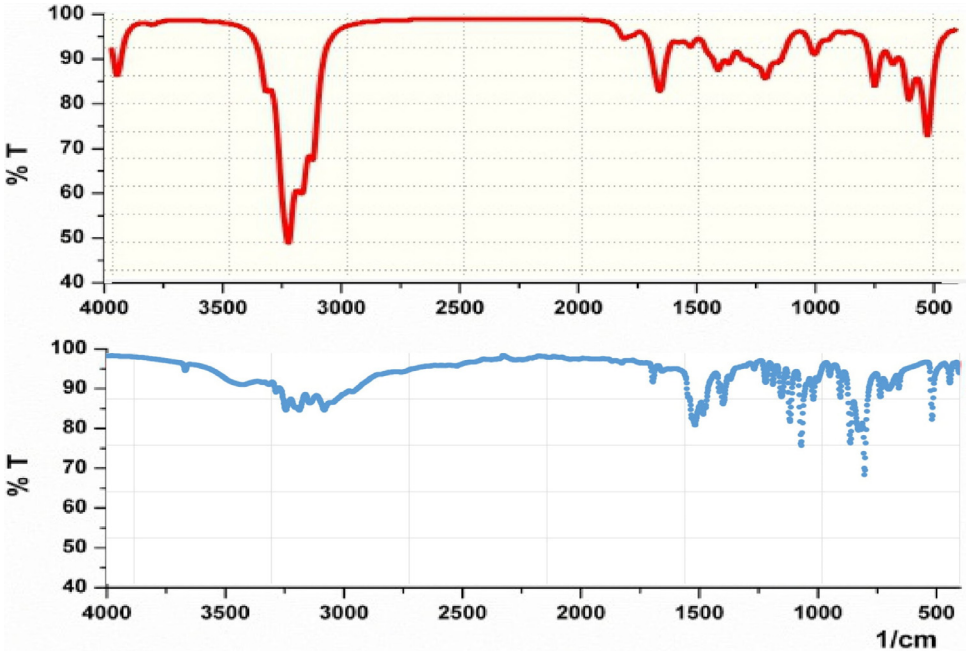

Fig. 14. IR spectra of compound **2**.

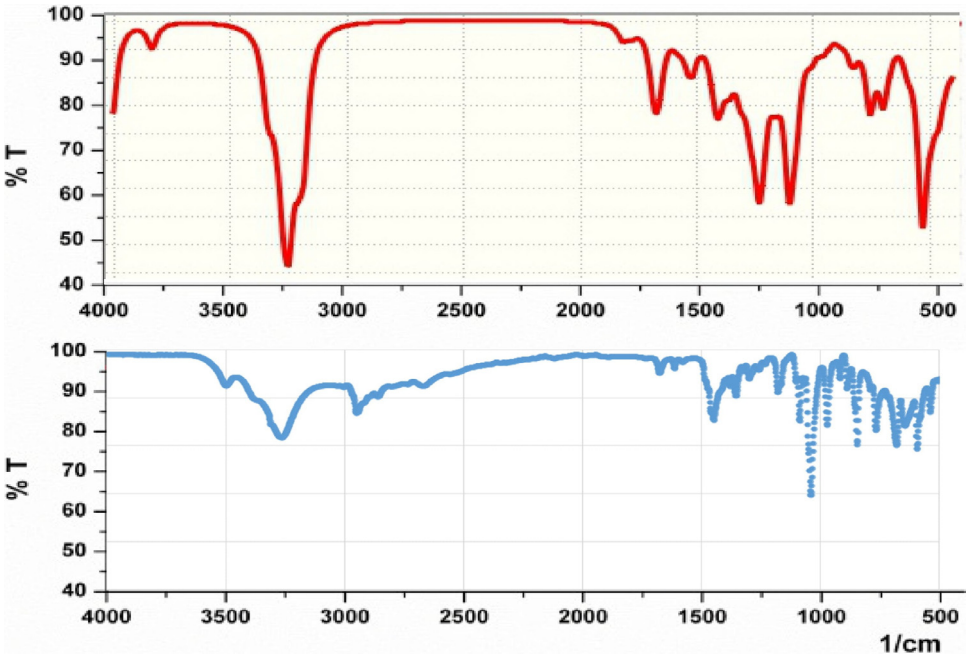

Fig. 15. IR spectra of compound **2**.

3.3. UV spectra

Ultraviolet and visible light (UV–Vis) absorption spectroscopy is the measurement of the attenuation of a beam of light after it has passed through a sample or is reflected off a sample surface. UV–Vis spectroscopy is generally used for the measurement of molecules in solution or inorganic ions and complexes [78]. Ultraviolet or ultraviolet (abbreviated UV) radiation is radiation with a wavelength between 100 and 400 nm. This spectroscopic method is used to determine the concentration of that substance or to determine the substance as a result of the substance absorbing light at certain wavelengths. In the calculations, compounds 1, 2, and 3 were found to be in gas (e = 1), chloroform (e = 4.711), methanol (e = 32.613), dimethyl sulfoxide (e = 46.826), water (e = 78.355), and n-methyl formamide-mixture (e = 181.56) phases were calculated. These phases of all compound are calculated on HF/6–31++g basis set in Figs. 16–18.

For the purpose of investigating the UV spectrum analyses of the molecules, they were studied by theoretical computation using the combined experimental results [77]. It was revealed that the examined peaks were located at 240 nm in compound 1, at 205, 220 and 230 nm in compound 2, and the absorption peaks of compound 3 were detected at 230 nm with a small excited peak at 205 nm. The highest absorption values recorded experimentally are 205 and 250 nm due to n $\rightarrow \pi*$ transition [78,79]. According to the above-mentioned observation, an infer-

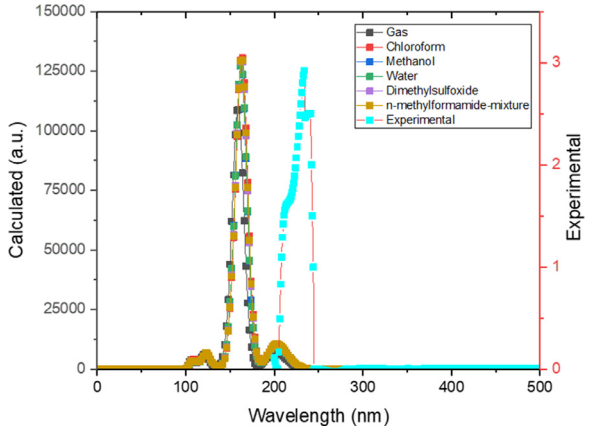

Fig. 16. UV–vis spectrum of compound **1**.

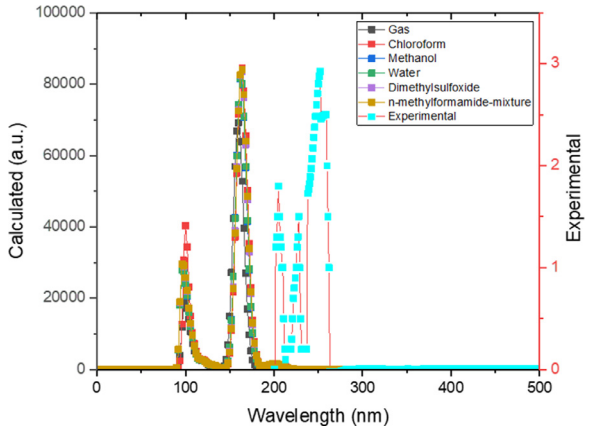

Fig. 17. UV–vis spectrum of compound **2**.

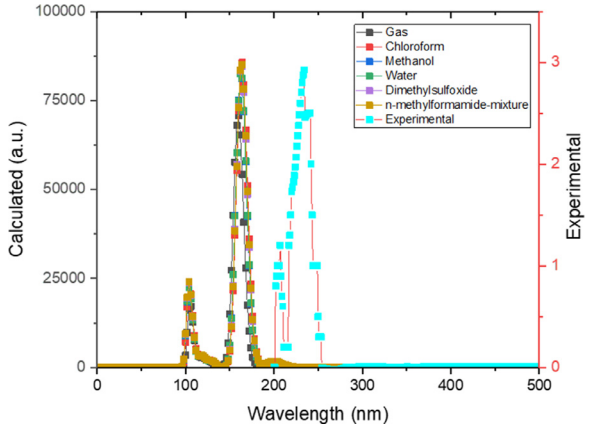

Fig. 18. UV–vis spectrum of compound **3**.

ence that all the peaks were identified with small fluctuations was made.

3.4. Molecular docking

Molecular docking calculations were used to compare the activity of molecules against biological materials. These calculations have important benefits in designing more active and more effective drugs for many diseases such as cancer. There are many factors affecting the activities of molecules in these calculations. At the very beginning of these factors, the inhibition of molecules by interacting with cancer proteins is the most important thing that affects the activities of molecules. Many chemical interactions occur between molecules and proteins, such as hydrogen bonds, polar and hydrophobic interactions, π-π and halogen [80,81].

Molecular docking calculations are made to predict the activity of molecules against biological materials. In molecular docking calculations, in order to be able to comment on the biological activities of molecules, it is necessary to examine the numerical value of the docking score parameter of the molecules, and it is known that the molecule with the most negative numerical value of this parameter has the highest activity [80]. The interactions of the molecule with the proteins are given in Fig. 19 and 20.

All parameters calculated as a result of the interaction of the molecules with the proteins are given in Table 3. Among these parameters, parameters such as Glide ligand efficiency, Glide hbond, Glide evdw, and Glide ecoul show the efficiency of the molecule and the numerical value of the chemical interactions in the interaction [80]. These chemical interactions are hydrogen bonds, polar and hydrophobic interactions, π-π and halogen. On the other hand, parameters such as Glide emodel, Glide energy, Glide einternal, and Glide posenum are the numerical values of the pose between the molecule and the protein [81].

While examining the interaction of the molecules with proteins, it was understood as a result of molecular docking calculations that compound 3 had higher activity than others. After the activity of the molecules, it is necessary to examine the drug properties so that the molecule can be used as a drug in the future [82]. ADME/T (Absorption, Distribution, Metabolism, Excretion and Toxicity) analysis was performed for these calculations in Table 4. This figure examines the entry of the molecule into human metabolism, its interaction in human metabolism, and a series of processes that follow excretion from human metabolism. All parameters obtained as a result of the calculations of this analysis are given in Table 6. Some of these parameters are about the chemical properties of the molecule and some of them are about the biological properties. However, there are two important parameters that determine whether molecules can be drugs, which are RuleOfFive [83,84], also known as Lipinski's fifth rule of Pfizer, and RuleOfThree [85], known as the three of Jorgensen's rule. The numerical value of these parameters is required to be zero. However, it is seen by theoretical calculations that the all compound is difficult to pass through the blood-brain and blood-intestinal barriers.

Table 3
Numerical values of the docking parameters of molecule against enzymes.

3PWH	Compound 1	Compound 2	Compound 3
Docking Score	−6.45	−7.79	−8.00
Glide ligand efficiency	−0.32	−0.52	−0.38
Glide hbond	0.00	−0.36	−1.06
Glide evdw	−31.40	−15.98	−15.09
Glide ecoul	−2.44	−15.18	−30.48
Glide emodel	−43.81	−53.82	−73.35
Glide energy	−33.83	−31.16	−45.57
Glide einternal	5.43	3.58	11.02
Glide posenum	73	370	211
5NM4	**Compound 1**	**Compound 2**	**Compound 3**
Docking Score	−6.33	−5.32	−6.58
Glide ligand efficiency	−0.32	−0.35	−0.27
Glide hbond	−0.32	−0.20	−0.30
Glide evdw	−26.11	−19.62	−20.76
Glide ecoul	−4.22	−8.97	−25.24
Glide emodel	−40.33	−44.12	−63.91
Glide energy	−30.33	−28.60	−46.00
Glide einternal	4.67	1.32	10.22
Glide posenum	338	248	248

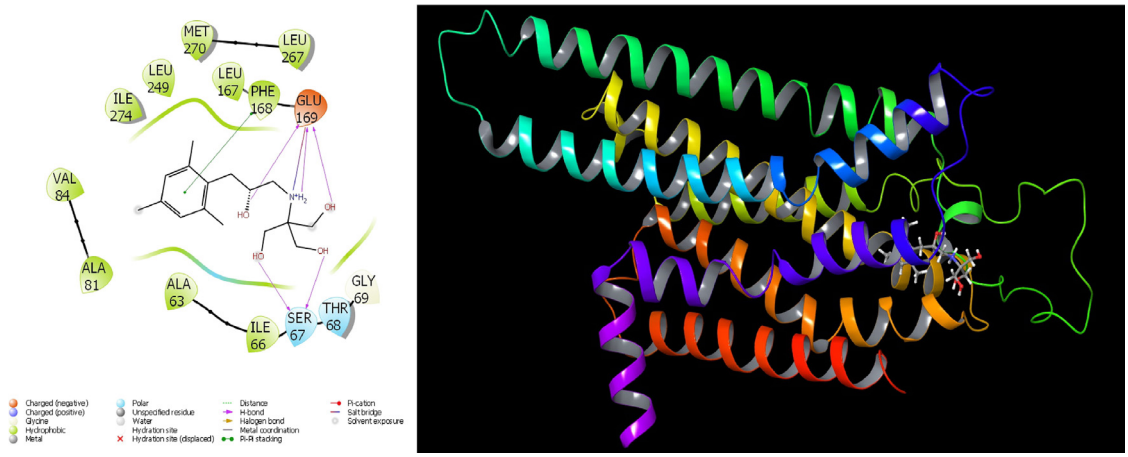

Fig. 19. Presentation interactions of Compound **3** with 3PWH protein.

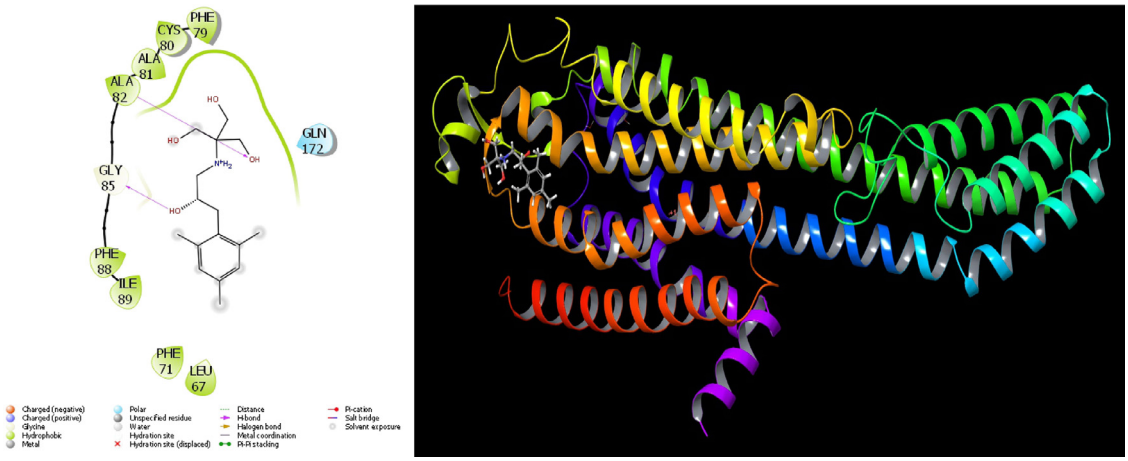

Fig. 20. Presentation interactions of Compound **3** with 5NM4 protein.

3.5. Enzymes results

The AChE plays a primary role in acetylcholine-mediated neurotransmission. At the therapeutic level, the utilization of AChE inhibitors is used to increase synaptic levels of acetylcholine in diseases that reduce acetylcholine neurotransmission, such as AD [86]. However, BChE activity regularly increments in patients with AD, while AChE action stays unaltered or decays. Both enzymes, therefore, represent right therapeutic targets for improving the cholinergic shortfall considered to be responsible for the declines in cognitive and behavioral characteristic of AD [87]. These compounds showed excellent to good inhibitory activities against studied AChE enzyme with K_i values ranging between 35.88±6.61 to 45.34±3.50 μM for AChE, whereas, tacrine, which was the first drug approved by the Food and Drug Administration for treatment of AD. It had K_i value of 117.48±23.61 μM against AChE (Table 5). The most potent compounds against AChE were order compounds **3, 2** and **1** with K_i values of 35.88±6.61, 43.75±8.28, and 45.34±3.50 μM against AChE, respectively. The order of IC_{50} inhibitory activity against AChE for these derivatives were **3** (32.73 μM) < **2** (38.82 μM) < **1** (44.64 μM). AChE inhibitors such as Donepezil and Rivastigmine are generally used for this purpose. However, it has been reported that these drugs cause side effects such as hepatotoxicity and gastrointestinal disorders. Therefore, safe and effective natural AChE inhibitors are gaining more and more importance recently. Competitive and non-competitive reversible AChE inhibitors are mostly used for therapeutic purposes [88]. These inhibitör compounds include carbamates, neostigmine, physostigmine, ambenonium, demecarium, pyridostigmine, phenanthrene derivatives, rivastigmine, galantamine, caffeine (non-competitive), donepezil, piperidines, tacrine (tetrahydroaminocri-

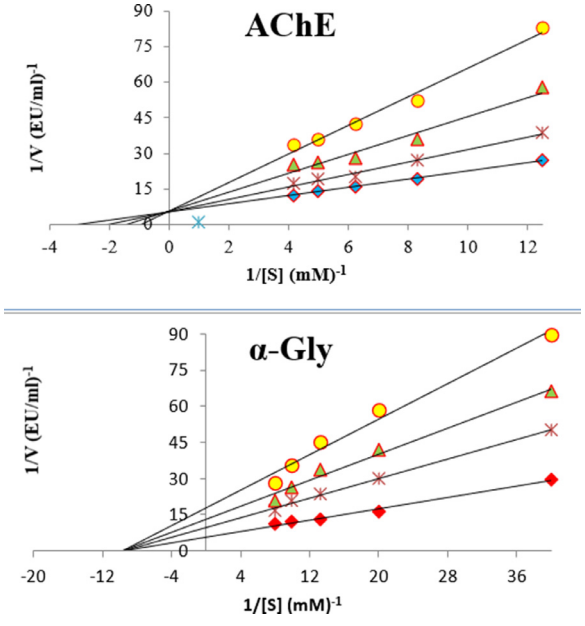

Fig. 21. Ki graphs of best inhibitor (**3**) for AChE and alpha glycosidase enzymes.

Table 4
ADME properties of molecules.

	Compound 1	Compound 2	Compound 3	Referance Range
mol_MW	269	207	297	130–725
dipole (D)	1.5	3.2	6.3	1.0–12.5
SASA	564	476	551	300–1000
FOSA	267	357	350	0–750
FISA	41	50	133	7–330
PISA	256	68	68	0–450
WPSA	0	0	0	0–175
volume (A^3)	981	805	994	500–2000
donorHB	2	2	5	0–6
accptHB	2.7	3.2	7.8	2.0–20.0
glob (Sphere =1)	0.8	0.9	0.9	0.75–0.95
QPpolrz (A^3)	31.7	23.5	26.6	13.0–70.0
QPlogPC16	9.9	7.0	10.1	4.0–18.0
QPlogPoct	14.2	11.6	20.1	8.0–35.0
QPlogPw	7.4	6.6	14.8	4.0–45.0
QPlogPo/w	4.2	1.2	0.5	−2.0–6.5
QPlogS	−4.4	−1.7	−0.6	−6.5–0.5
ClQPlogS	−4.2	−1.4	−1.5	−6.5–0.5
QPlogHERG	−5.2	−4.5	−4.6	*
QPPCaco (nm/*sec*)	4012	830	136	**
QPlogBB	−0.2	0.2	−0.9	−3.0–1.2
QPPMDCK (nm/*sec*)	2221	448	63	**
QPlogKp	−0.8	−3.8	−4.6	Kp in cm/hr
IP (ev)	8.3	9.0	8.9	7.9–10.5
EA (eV)	−0.4	−0.5	−0.7	−0.9–1.7
#metab	8	6	9	1–8
QPlogKhsa	0.4	−0.1	−0.6	−1.5–1.5
Human Oral Absorption	3	3	2	–
Percent Human Oral Absorption	100	86	68	***
PSA	30	31	87	7–200
RuleOfFive	0	0	0	Maximum is 4
RuleOfThree	1	0	1	Maximum is 3
Jm	1.7	0.7	1.9	–

* Corcern below −5.
** <25 is poor and >500 is great.
*** <25% is poor and >80% is high.

Table 5
The enzyme inhibition results of novel compounds (**1–3**) against acetylcholinesterase and α-glycosidase enzymes.

Compounds			IC_{50} (μM)		Ki (μM)	
	AChE	r^2	α-Gly	r^2	AChE	α-Gly
1	44.64	0.9828	1.05	0.9885	45.34±3.50	1.32±0.32
2	38.82	0.9961	0.93	0.9721	43.75±8.28	1.06±0.31
3	32.73	0.9883	0.16	0.9824	35.88±6.61	0.12±0.03
TAC**	125.27	0.9921	–	–	117.48±23.61	–
ACR***	–	–	22.80	0.9391	–	12.60±1.81

** TAC (tacrine) was used as a positive control for acetylcholinesterase (AChE).
*** Acarbose was used as a positive control for α-glycosidase enzyme. This has given in references [90,91].

dine, THA), huperophonymine, edrophonium, lalactuungados that we can write example. AChE enzyme inhibitors are used in many fields. These areas are listed below. (a) Naturally, venoms of plant and animal origin can inhibit the AChE enzyme. (b) They are found in insecticides. (c) For medical purposes, it is used in the treatment of glaucoma and myasthenia gravis [89].

Finally, α-glucosidase inhibitory activity of the derivatives was determined in this study (Table 5). Also, obtained results demonstrated that all these compounds (K_i values = 0.12±0.03–1.32±0.32 μM) acted better than standard inhibitor acarbose (K_i value = 12.60±0.78 μM) against α-glucosidase. The most active compounds were order **3, 2,** and **1** that had K_i values 3 (0.12) < 2 (1.06) ≤ 1 (1.32) μM in Fig. 21. α-glucosidase inhibitors are compounds from the oral antidiabetic class used in the treatment of Type 2 diabetes. These groups of compounds inhibit the conversion of carbohydrates to monosaccharides, reducing their absorption by the intestine [92]. Thus, α-glucosidase inhibitors decrease blood glucose level and insulin level. When we look at the literature, synthesized a group of new benzimidazole derivatives and conducted inhibition studies on yeast α-glucosidase.

4. Conclusion

In conclusion, a series of novel β-amino alcohol compounds **1–3** has been designed, synthesized, and evaluated against metabolic enzymes AchE and α-glucosidase. All of the synthesized compounds inhibited AChE and alpha glycosidase better than positive control tacrin and acarbose. Among them, 2-((2-Hydroxy-3-mesitylpropyl)amino)−2-(hydroxymethyl)propane-1,3-diol **(3)** derivative showed the most potent anti-AChE and

alpha glycosidase activities. Interestingly, compound 1-Mesityl-3-(methylamino)propan-2-ol **(2)** was the second potent compound against AChE and α-glucosidase activities. All the title compounds **1–3** with K_i values in range of 35 to 46 µM for AChE were excellent inhibitors in comparison positive control tacrine with K_i value of 117.5. Consequently, it was determined that the compounds were more effective in neuroblastoma cells. Cholinesterase inhibitors function to decrease the breakdown of acetylcholine that use in the treatment of Alzheimer and dementia symptoms. Additionally, Alpha-glucosidase inhibitors are oral anti-diabetic drugs used for diabetes mellitus type 2 that work by preventing the digestion of carbohydrates (such as starch and table sugar). We think that the compounds may be drug nominees with the support of in vitro and in vivo studies in the future.

Declaration of Competing Interest

The authors declare that they have no known competing financial interests or personal relationships that could have appearedto influence the work reported in this paper.

CRediT authorship contribution statement

Ayca Tas: Investigation. **Burak Tüzün:** Software, Investigation, Writing – original draft, Writing – review & editing. **Ali N. Khalilov:** Investigation, Writing – original draft, Writing – review & editing. **Parham Taslimi:** Investigation, Writing – original draft, Writing – review & editing. **Nese Keklikcioglu Cakmak:** Investigation.

Data Availability

No data was used for the research described in the article.

Acknowledgements

The numerical calculations reported in this paper were fully/partially performed at TUBITAK ULAKBIM, High Performance and Grid Computing Center (TRUBA resources). This work was supported by the Scientific Research Project Fund of Sivas Cumhuriyet University (CUBAP) under the project number RGD-020.

Supplementary materials

Supplementary material associated with this article can be found, in the online version, at doi:10.1016/j.molstruc.2022.134282.

References

[1] H.S. Lee, S.H. Kang, Synthesis of physiologically potent β-amino alcohols, Synlett 10 (2004) 1673–1685.
[2] U.V.S. Reddy, M. Chennapuram, C. Seki, E. Kwon, Y. Okuyama, H. Nakano, Catalytic Efficiency of Primary β-Amino Alcohols and Their Derivatives in Organocatalysis, Eur. J. Org. Chem. 24 (2016) 4124–4143.
[3] C.P. Pradeep, S.K. Das, Coordination and supramolecular aspects of the metal complexes of chiral N-salicyl-β-amino alcohol Schiff base ligands: towards understanding the roles of weak interactions in their catalytic reactions, Coord. Chem. Rev. 257 (11–12) (2013) 1699–1715.
[4] D.J. Ager, I. Prakash, D.R. Schaad, 1, 2-Amino alcohols and their heterocyclic derivatives as chiral auxiliaries in asymmetric synthesis, Chem. Rev. 96 (2) (1996) 835–876.
[5] J. Cossy, D.G. Pardo, C. Dumas, O. Mirguet, I. Dechamps, T.X. Métro, … A. Cochi, Rearrangement of β-amino alcohols and application to the synthesis of biologically active compounds, Chirality: Pharmacol. Biol. Chem. Consequences Mol. Asymmetry 21 (9) (2009) 850–856.
[6] D. Bhagavathula, G. Boddeti, V. Reddy, A brief review on synthesis of β-amino alcohols by ring opening of epoxides, Res. Rev. J. Chem 6 (2017) 27–46.
[7] A. Viswanathan, D. Kute, A. Musa, S.K. Mani, V. Sipilä, F. Emmert-Streib, … M. Kandhavelu, 2-(2-(2, 4-dioxopentan-3-ylidene) hydrazineyl) benzonitrile as novel inhibitor of receptor tyrosine kinase and PI3K/AKT/mTOR signaling pathway in glioblastoma, Eur. J. Med. Chem. 166 (2019) 291–303.
[8] S.J. Kwon, S.Y. Ko, Synthesis of statine employing a general syn-amino alcohol building block, Tetrahedron Lett. 43 (4) (2002) 639–641.
[9] C.U. Ingram, M. Bommer, M.E.B. Smith, P.A. Dalby, J.M. Ward, H.C. Hailes, G.J. Lye, One-pot synthesis of amino-alcohols using a de-novo transketolase and β-alanine: pyruvate transaminase pathway in Escherichia coli, Biotechnol. Bioeng. 96 (3) (2007) 559-569.
[10] M. Quiliano, A. Mendoza, K.Y. Fong, A. Pabón, N.E. Goldfarb, I. Fabing, … S. Galiano, Exploring the scope of new arylamino alcohol derivatives: synthesis, antimalarial evaluation, toxicological studies, and target exploration, Int. J. Parasitol. Drugs Drug Resist. 6 (3) (2016) 184–198.
[11] A.M. De Almeida, T. Nascimento, B.S. Ferreira, P.P. de Castro, V.L. Silva, C.G. Diniz, M. Le Hyaric, Synthesis and antimicrobial activity of novel amphiphilic aromatic amino alcohols, Bioorg. Med. Chem. Lett. 23 (10) (2013) 2883–2887.
[12] Y. El Ouadi, M. Manssouri, A. Bouyanzer, L. Majidi, B. Hammouti, Essential oil composition and antifungal activity of Melissa officinalis originating from north-Est Morocco, against postharvest phytopathogenic fungi in apples, Microb. Pathog. 107 (2017) 321–326.
[13] A. El Moussaoui, F.Z. Jawhari, A.M. Almehdi, H. Elmsellem, A. Bari, Antibacterial, antifungal and antioxidant activity of total polyphenols of Withania frutescens. L, Bioorg. Chem. 93 (2019) 103337.
[14] A. I. Maliki, A. Moussaoui, M. Ramdani, K. El Badaoui, Phytochemical screening and the antioxidant, antibacterial and antifungal activities of aqueous extracts from the leaves of Salvia officinalis planted in Morocco, Moroccan J. Chem. 9 (2) (2021) 354–368.
[15] N.A. Minton, A.R. Baird, J.A. Henry, Modulation of the effects of salbutamol by propranolol and atenolol, Eur. J. Clin. Pharmacol. 36 (5) (1989) 449–453.
[16] A.V. Zakharov, E.V. Varlamova, A.A. Lagunin, A.V. Dmitriev, E.N. Muratov, D. Fourches, … M.C. Nicklaus, Qsar modeling and prediction of drug–drug interactions, Mol. Pharm. 13 (2) (2016) 545–556.
[17] C. Teixeira, N.F. Pinto, D.M. Pereira, R.B. Pereira, M.J.G. Fernandes, E. Castanheira, … M.S.T. Gonçalves, Cytotoxicity studies of eugenol amino alcohols derivatives, Chem. Proc. 8 (1) (2021) 105.
[18] J.R. Baker, C.C. Russell, J. Gilbert, A. McCluskey, J.A. Sakoff, Amino alcohol acrylonitriles as broad spectrum and tumour selective cytotoxic agents, RSC Med. Chem. 12 (6) (2021) 929–942.
[19] A.M. Magerramov, A.N. Khalilov, M.A. Allahverdiyev, I.G. Mammadov, G.A. Aliyeva, Synthesis of some arylsubstituted 1,2-aminoalcohols on the base of 1-(2′,4′,6′-trimethyfenyl)-3-chloropropanole, Chem. Probl. 1 (2006) 122–126.
[20] C. Ploessl, A. Pan, K.T. Maples, D.K. Lowe, Dinutuximab: an anti-GD2 monoclonal antibody for high-risk neuroblastoma, Ann. Pharmacother. 50 (5) (2016) 416–422.
[21] J.L. Young Jr, L.G. Ries, E. Silverberg, J.W. Horm, R.W Miller, Cancer incidence, survival, and mortality for children younger than age 15 years, Cancer 58 (1986) 598–602.
[22] P. Voute, Neuroblastoma, in: W. Sutow, D. Fernbach, T. Vietti (Eds.), Clincal Pediatric Oncology, Mosby, CV, St. Louis, 1984, p. 559.
[23] M.A. Bonilla, N.K.V. Cheung, Clinical progress in neuroblastoma, Cancer Invest. 12 (6) (1994) 644–653.
[24] K.K. Matthay, J.M. Maris, G. Schleiermacher, A. Nakagawara, C.L. Mackall, L. Diller, W.A. Weiss, Neuroblastoma, Nat. Rev. Dis. Primers 2 (2016) 16078.
[25] G.M. Brodeur, R. Iyer, J.L. Croucher, T. Zhuang, M. Higashi, V. Kolla, Therapeutic targets for neuroblastomas, Expert Opin. Ther. Targets 18 (3) (2014) 277–292.
[26] H. Bendaif, A. Melhaoui, M. Ramdani, H. Elmsellem, Y. El Ouadi, Antibacterial activity and virtual screening by molecular docking of lycorine from Pancratium foetidum Pom (Moroccan endemic Amaryllidaceae), Microb. Pathog. 115 (2018) 138–145.
[27] M. Dahmani, A. Ettouhami, B. El Bali, A. Yahyi, C. Wilson, K. Ullah, R. Imad, S. Ullah, S. Wajid, F. Arshad, H. Elmsellem, Organotin (IV) derivative of Piperic acid and Phenylthioacetic acid: synthesis, Crystal structure, Spectroscopic characterizations and Biological activities, Mor. J. Chem. 8 (1) (2020) 244–263.
[28] M.J. Frisch, G.W. Trucks, H.B. Schlegel, G.E. Scuseria, M.A. Robb, J.R. Cheeseman, G. Scalmani, V. Barone, B. Mennucci, G.A. Petersson, H. Nakatsuji, M. Caricato, X. Li, H.P. Hratchian, A.F. Izmaylov, J. Bloino, G. Zheng, J.L. Sonnenberg, M. Hada, M. Ehara, K. Toyota, R. Fukuda, J. Hasegawa, M. Ishida, T. Nakajima, Y. Honda, O. Kitao, H. Nakai, T. Vreven, J.A. Montgomery, J.E. Peralta, F. Ogliaro, M. Bearpark, J.J. Heyd, E. Brothers, K.N. Kudin, V.N. Staroverov, R. Kobayashi, J. Normand, K. Raghavachari, A. Rendell, J.C. Burant, S.S. Iyengar, J. Tomasi, M. Cossi, N. Rega, J.M. Millam, M. Klene, J.E. Knox, J.B. Cross, V. Bakken, C. Adamo, J. Jaramillo, R. Gomperts, R.E. Stratmann, O. Yazyev, A.J. Austin, R. Cammi, C. Pomelli, J.W. Ochterski, R.L. Martin, K. Morokuma, V.G. Zakrzewski, G.A. Voth, P. Salvador, J.J. Dannenberg, S. Dapprich, A.D. Daniels, O. Farkas, J.B. Foresman, J.V. Ortiz, J. Cioslowski, D.J. Fox, Gaussian 09, Revision D.01, Gaussian Inc, Wallingford CT, 2009.
[29] Schrödinger Release 2021-3: Maestro, Schrödinger, LLC, New York, NY, 2021.
[30] M. Rezaeivala, S. Karimi, B. Tuzun, K. Sayin, Anti-corrosion behavior of 2-((3-(2-morpholino ethylamino)-N3-((pyridine-2-yl) methyl) propylimino) methyl) pyridine and its reduced form on Carbon Steel in Hydrochloric Acid solution: experimental and theoretical studies, Thin. Solid. Films (2021) 139036.
[31] K. Karrouchi, S. Fettach, B. Tüzün, S. Radi, A.I. Alharthi, H.A. Ghabbour, … Y. Garcia, Synthesis, crystal structure, DFT, α-glucosidase and α-amylase inhibition and molecular docking studies of (E)-N'-(4-chlorobenzylidene)-5-phenyl-1H-pyrazole-3-carbohydrazide, J. Mol. Struct. 1245 (2021) 131067.
[32] A.D. Becke, Density-functional thermochemistry. I. The effect of the exchange-only gradient correction, J. Chem. Phys. 96 (3) (1992) 2155–2160.

[33] D. Vautherin, D.T. Brink, Hartree-Fock calculations with Skyrme's interaction. I. Spherical nuclei, Phys. Rev. C 5 (3) (1972) 626.
[34] E.G. Hohenstein, S.T. Chill, C.D. Sherrill, Assessment of the performance of the M05− 2X and M06− 2X exchange-correlation functionals for noncovalent interactions in biomolecules, J. Chem. Theory Comput. 4 (12) (2008) 1996–2000.
[35] A.S. Doré, N. Robertson, J.C. Errey, I. Ng, K. Hollenstein, B. Tehan, … F.H. Marshall, Structure of the adenosine A2A receptor in complex with ZM241385 and the xanthines XAC and caffeine, Structure 19 (9) (2011) 1283–1293.
[36] T. Weinert, N. Olieric, R. Cheng, S. Brünle, D. James, D. Ozerov, … J. Standfuss, Serial millisecond crystallography for routine room-temperature structure determination at synchrotrons, Nat. Commun. 8 (1) (2017) 1–11.
[37] H. Genc Bilgicli, A. Kestane, P. Taslimi, O. Karabay, A. Bytyqi-Damoni, M. Zengin, İ. Gulçin, Novel eugenol bearing oxypropanolamines: synthesis, characterization, antibacterial, antidiabetic, and anticholinergic potentials, Bioorg. Chem. 88 (2019) 102931.
[38] P. Taslimi, F.M. Kandemir, Y. Demir, M. İleritürk, Y. Temel, C. Cağlayan, İ. Gülçin, The antidiabetic and anticholinergic effects of chrysin on cyclophosphamide-induced multiple organs toxicity in rats: pharmacological evaluation of some metabolic enzymes activities, J. Biochem. Mol. Toxicol. 33 (6) (2019) e22313.
[39] F. Erdemir, D. Barut Celepci, A. Aktaş, Y. Gök, R. Kaya, P. Taslimi, Y. Demir, İ. Gülçin, Novel 2-aminopyridine liganded Pd(II) N-heterocyclic carbene complexes: synthesis, characterization, crystal structure and bioactivity properties, Bioorg. Chem. 91 (2019) 103134.
[40] F. Turkan, A. Cetin, P. Taslimi, M. Karaman, İ. Gülçin, Synthesis, biological evaluation and molecular docking of novel pyrazole derivatives as potent carbonic anhydrase and acetylcholinesterase inhibitors, Bioorg. Chem. 86 (2019) 420–427.
[41] A.M. Maharramov, A.N. Khalilov, A.V. Gurbanov, M.A. Allahverdiyev, S.W. Ng, 1-Methylamino-3-(2, 4, 6-trimethylphenyl) propan-2-ol, Acta Crystallogr. Sect. E Struct. Rep. Online 67 (4) (2011) o784-o784.
[42] R. Dennington, T.A. Keith, J.M. Millam, GaussView 6.0. 16, Semichem Inc., Shawnee Mission, KS, USA, 2016.
[43] M.B. Gürdere, Y. Budak, U.M. Kocyigit, P. Taslimi, B. Tüzün, M. Ceylan, ADME properties, bioactivity and molecular docking studies of 4-amino-chalcone derivatives: new analogues for the treatment of Alzheimer, glaucoma and epileptic diseases, In Silico Pharmacol. 9 (1) (2021) 1–11.
[44] A. Şenocak, N.A. Taş, P. Taslimi, B. Tüzün, A. Aydin, A. Karadağ, Novel amino acid Schiff base Zn (II) complexes as new therapeutic approaches in diabetes and Alzheimer's disease: synthesis, characterization, biological evaluation, and molecular docking studies, J. Biochem. Mol. Toxicol. (2021) e22969.
[45] A. Poustforoosh, S. Faramarz, M.H. Nematollahi, H. Hashemipour, B. Tüzün, A. Pardakhty, M. Mehrabani, 3D-QSAR, molecular docking, molecular dynamics, and ADME/T analysis of marketed and newly designed flavonoids as inhibitors of Bcl-2 family proteins for targeting U-87 glioblastoma, J. Cell. Biochem. (2021).
[46] Schrödinger Release 2019-4: Protein Preparation Wizard; Epik, Schrödinger, LLC, New York, NY, 2016; Impact, Schrödinger, LLC, New York, NY, 2016; Prime, Schrödinger, LLC, New York, NY, 2019.
[47] Schrödinger Release 2021-3: LigPrep, Schrödinger, LLC, New York, NY, 2021.
[48] P. Taslimi, Y. Demir, H.E. Duran, Ü.M. Koçyiğit, B. Tüzün, O.N. Aslan, … İ. Gülçin, Some old 2-(4-(Aryl)-thiazole-2-yl)-3a, 4, 7, 7a-tetrahydro-1H-4, 7-tethanoisoindole-1, 3 (2H)-dione derivatives: synthesis, inhibition effects and molecular docking studies on Aldose reductase and α-Glycosidase, Cumhuriyet Sci. J. 42 (3) (2021) 553–564.
[49] Schrödinger Release 2021-3, QikProp, Schrödinger, LLC, New York, NY, 2021.
[50] G.L. Ellman, K.D. Courtney, V. Andres Jr,, R.M. Featherstone, A new and rapid colorimetric determination of acetylcholinesterase activity, Biochem. Pharmacol. 7 (2) (1961) 88–95.
[51] K. Küçükoğlu, H.İ. Gül, P. Taslimi, İ. Gülçin, C.T. Supuran, Investigation of inhibitory properties of some hydrazone compounds on hCA I, hCA II and AChE enzymes, Bioorg. Chem. 86 (2019) 316–321.
[52] Y. Tao, Y. Zhang, Y. Cheng, Y. Wang, Rapid screening and identification of α-glucosidase inhibitors from mulberry leaves using enzyme-immobilized magnetic beads coupled with HPLC/MS and NMR, Biomed. Chromatogr. 27 (2) (2013) 148–155.
[53] A. Riccardi, T. Servidei, A. Tornesello, P. Puggioni, S. Mastrangelo, C. Rumi, R. Riccardi, Cytotoxicity of paclitaxel and docetaxel in human neuroblastoma cell lines, Eur. J. Cancer 31 (4) (1995) 494–499.
[54] P. Taslimi, F. Akhundova, M. Kurbanova, F. Türkan, B. Tuzun, A. Sujayev, … İ. Gülçin, Biological activity and molecular docking study of some bicyclic structures: antidiabetic and anticholinergic potentials, Polycycl. Aromat. Compd. (2021) 1–14.
[55] M.T. Riaz, M. Yaqub, Z. Shafiq, A. Ashraf, M. Khalid, P. Taslimi, … İ. Gulçin, Synthesis, biological activity and docking calculations of bis-naphthoquinone derivatives from Lawsone, Bioorg. Chem. 114 (2021) 105069.
[56] M. Rbaa, A. Oubihi, H. Hajji, B. Tüzün, A. Hichar, E. Berdimurodov, … B. Lakhrissi, Synthesis, bioinformatics and biological evaluation of novel pyridine based on 8-hydroxyquinoline derivatives as antibacterial agents: DFT, molecular docking and ADME/T studies, J. Mol. Struct. (2021) 130934.
[57] M. Safa Çelik, Ş.A. Çetinus, A.F. Yenidünya, S. Çetinkaya, B. Tüzün, Biosorption of Rhodamine B dye from aqueous solution by Rhus coriaria L. plant: equilibrium, kinetic, thermodynamic and DFT calculations, J. Mol. Struct. (2022) 134158.
[58] B. Tüzün, K. Sayin, Investigations over optical properties of boron complexes of benzothiazolines, Spectrochim. Acta, Part A 208 (2019) 48–56.
[59] M. Akin, A. Günsel, A.T. Bilgicli, B. Tüzün, G. Arabaci, N. Şaki, M.N. Yarasir, The Water-Soluble Peripheral Substituted Phthalocyanines as Corrosion Inhibitors for Copper in 0.1N HCl: gravimetric, Electrochemical, SEM-EDS, and Quantum Chemical Calculations, Protect. Metals Phys. Chem. Surfaces 56 (3) (2020) 609–618.
[60] A.T. Bilgicli, H.G. Bilgiçli, A. Günsel, H. Pişkin, B. Tüzün, M.N. Yarasir, M. Zengin, The new ball-type zinc phthalocyanine with SS bridge; Synthesis, computational and photophysicochemical properties, J. Photochem. Photobiol. 389 (2020) 112287.
[61] A. Günsel, A. Kobyaoğlu, A.T. Bilgicli, B. Tüzün, B. Tosun, G. Arabaci, M.N. Yarasir, Novel biologically active metallophthalocyanines as promising antioxidant-antibacterial agents: synthesis, characterization and computational properties, J. Mol. Struct. 1200 (2020) 127127.
[62] H. Genç Bilgiçli, P. Taslimi, B. Akyuz, B. Tuzun, I Gulcin, Synthesis, characterization, biological evaluation, and molecular docking studies of some piperonyl-based 4-thiazolidinone derivatives, Arch. Pharm. (Weinheim) 353 (1) (2020) 1900304.
[63] A. Günsel, A.T. Bilgiçli, B. Tüzün, H. Pişkin, M.N. Yarasir, B. Gündüz, Optoelectronic parameters of peripherally tetra-substituted copper (ii) phthalocyanines and fabrication of a photoconductive diode for various conditions, New J. Chem. 44 (2) (2020) 369–380.
[64] A.A. Manthiri, S. Ramalingam, G. George, R. Aarthi, Molecular structure analysis and biological properties investigation on antiseptic drug; 2-amino-1-phenyl-1-propanol using spectroscopic and computational research analysis, Heliyon 7 (4) (2021) e06699.
[65] N.B. Colthup, L.H. Daly, S.E. Wiberley, Introduction to Infrared and Raman Spectroscopy, Academic Press, New York, 1964.
[66] R.M. Silverstein, G.C. Bassler, Spectrometric identification of organic compounds, J. Chem. Educ. 39 (11) (1962) 546.
[67] V. Arjunan, I. Saravanan, P. Ravindran, S. Mohan, Ab initio, density functional theory and structural studies of 4-amino-2-methylquinoline, Spectrochim. Acta, Part A 74 (2) (2009) 375–384.
[68] E. Kose, A. Atac, M. Karabacak, P.B. Nagabalasubramanian, A.M. Asiri, S. Periandy, FT-IR and FT-Raman, NMR and UV spectroscopic investigation and hybrid computational (HF and DFT) analysis on the molecular structure of mesitylene, Spectrochim. Acta, Part A 116 (2013) 622–634.
[69] M.K. Rofouei, N. Sohrabi, M. Shamsipur, E. Fereyduni, S. Ayyappan, N. Sundaraganesan, X-ray crystallography characterization, vibrational spectroscopy, NMR spectra and quantum chemical DFT/HF study of N, N′-di (2-methoxyphenyl) formamidine, Spectrochim. Acta, Part A 76 (2) (2010) 182–190.
[70] H.F. Hameka, J.O. Jensen, Theoretical studies of the methyl rotational barrier in toluene, J. Mol. Struct. 362 (3) (1996) 325–330.
[71] V. Krishnakumar, S. Dheivamalar, Density functional theory study of Fourier transform infrared and Raman spectra of 2-amino-5-chloro benzonitrile, Spectrochim. Acta, Part A 71 (2) (2008) 465–470.
[72] N.P.G. Roeges, A Guide to the Complete Interpretation of Infrared Spectra of Organic Structures, John Wiley and Sons Inc., New York, 1994.
[73] G. Socrate, Infrared Characteristic Group Frequencies G., John Wiley and Sons, New York, 1981.
[74] G. Varsányi, Assignments For Vibrational Spectra of Seven Hundred Benzene Derivatives, John Wiley & Sons, 1974 (Vol. 1).
[75] S.S. Fa, R.K. Sa, S.M. Yb, C.Y. Panickera, B Harikumarc, FT-IR, FT-Raman, NLO, MEP, NBO and Molecular docking study of 2-phenyl-1-propanol, Sci. Lett. 4 (2015) 202.
[76] H.T. Varghese, C.Y. Panicker, D. Philip, J.R. Mannekutla, S.R. Inamdar, IR, Raman and SERS studies of methyl salicylate, Spectrochim. Acta, Part A 66 (4–5) (2007) 959–963.
[77] F.A. Cotton, G. Wilkinson, C.A. Murillo, M. Bochmann, R. Grimes, in: Advanced Inorganic Chemistry, Wiley, New York, 1988, p. 1455. Vol. 6.
[78] A. Günsel, A.T. Bilgiçli, H. Pişkin, B. Tüzün, N.Ç. Delibaş, M.N. Yarasir, B. Gündüz, Comparison of spectroscopic, electronic, theoretical, optical and surface morphological properties of functional manganese (III) phthalocyanine compounds for various conditions, J. Mol. Struct. 1193 (2019) 247–264.
[79] A. Günsel, A.T. Bilgiçli, H. Pişkin, B. Tüzün, M.N. Yarasir, B. Gündüz, Synthesis of non-peripherally tetra-substituted copper (ii) phthalocyanines: characterization, optical and surface properties, fabrication and photo-electrical properties of a photosensitive diode, Dalton Trans. 48 (39) (2019) 14839–14852.
[80] A. Aktaş, B. Tüzün, R. Aslan, K. Sayin, H. Ataseven, New anti-viral drugs for the treatment of COVID-19 instead of favipiravir, J. Biomol. Struct. Dyn. (2020) 1–11.
[81] A. Aktaş, B. Tüzün, H.A. Taşkın Kafa, K. Sayin, H. Ataseven, Clarification of interaction mechanism of arbidol with covid-19 and investigation of the inhibition activity analogues against covid-19, Bratisl. Lek. Listy 121 (10) (2020) 705–711.
[82] H. Genc Bilgicli, A. Kestane, P. Taslimi, O. Karabay, A. Bytyqi-Damoni, M. Zengin, İ. Gulçin, Novel eugenol bearing oxypropanolamines: synthesis, characterization, antibacterial, antidiabetic, and anticholinergic potentials, Bioorg. Chem. 88 (2019) (2019) 102931.
[83] C.A. Lipinski, Lead-and drug-like compounds: the rule-of-five revolution, Drug Discov. Today Technol. 1 (4) (2004) 337–341.
[84] C.A. Lipinski, F. Lombardo, B.W. Dominy, P.J. Feeney, Experimental and computational approaches to estimate solubility and permeability in drug discovery and development settings, Adv. Drug. Deliv. Rev. 23 (1997) 3–25.
[85] W.J. Jorgensen, E.M. Duffy, Prediction of drug solubility from structure, Adv. Drug. Deliv. Rev. 54 (3) (2002) 355–366.
[86] Ç. Bayrak, P. Taslimi, H.S. Kahraman, İ. Gülçin, A. Menzek, The first synthesis, carbonic anhydrase inhibition and anticholinergic activities of some bro-

mophenol derivatives with S including natural products, Bioorg. Chem. 85 (2019) 128–139.
[87] A. Biçer, P. Taslimi, G. Yakalı, İ. Gülcin, M.S. Gültekin, G.T. Cin, Synthesis, characterization, crystal structure of novel bis-thiomethylcyclohexanone derivatives and their inhibitory properties against some metabolic enzymes, Bioorg. Chem. 2019 (82) (2019) 393–404.
[88] M. Huseynova, A. Medjidov, P. Taslimi, M. Aliyeva, Synthesis, characterization, crystal structure of the coordination polymer zn(ii) with thiosemicarbazone of glyoxalic acid and their inhibitory properties against some metabolic enzymes, Bioorg. Chem. 2019 (83) (2019) 55–62.
[89] M. Huseynova, P. Taslimi, A. Medjidov, V. Farzaliyev, M. Aliyeva, G. Gondolova, O. Şahin, B. Yalçın, A. Sujayev, E.B. Orman, A.R. Özkaya, İ. Gülçin, Synthesis, characterization, crystal structure, electrochemical studies and biological evaluation of metal complexes with thiosemicarbazone of glyoxylic acid, Polyhedron 155 (2018) 25–33.
[90] M. Özil, M. Emirik, S.Y. Etlik, S. Ülker, B. Kahveci, A simple and efficient synthesis of novel inhibitors of alpha-glucosidase based on benzimidazole skeleton and molecular docking studies, Bioorg. Chem. 68 (2016) 226–235.
[91] H. Teng, L. Chen, T. Fang, B. Yuan, Q. Lin, Rb2 inhibits α-glucosidase and regulates glucose metabolism by activating AMPK pathways in HepG2 cells, J. Funct. Foods 28 (2017) 306–313.
[92] P. Taslimi, H.E. Aslan, Y. Demir, N. Oztaskin, A. Maraş, İ. Gulçin, … B. Diarilmethanon, Diarilmetan compounds: discovery of potent aldose reductase, α-amylase and α-glycosidase inhibitors as new therapeutic approach in diabetes and functional hyperglycemia, Int. J. Biol. Macromol. 119 (2018) 857–863.